Spatially periodic modulated Rayleigh-Bénard convection

R. Schmitz and W. Zimmermann
Institut für Festkörperforschung, Forschungszentrum Jülich, D-52425 Jülich, Federal Republic of Germany
(Received 30 November 1995)

Two-dimensional thermal convection in a fluid layer between two rigid walls at different mean temperatures is investigated. The top container boundary is undulated and the temperatures at the top and bottom boundaries are spatially periodic modulated, with modulation wavelengths large compared to the thickness of the fluid layer. The continuous translational invariance in the fluid layer is broken by these spatial modulations. Consequently phase differences between two periodic modulations give rise to an interesting drifting pattern, with the drift direction depending on the sign of the relative phase between the modulations. At distinguished ratios between the modulation wave numbers and relative phases the onset of convection changes as function of the modulation amplitudes from a stationary into an oscillatory one: We call this phenomenon *Hopf bifurcation by frustrated drifts*. Possible experiments are described in detail where this phenomenon can be expected. [S1063-651X(96)05805-5]

PACS number(s): 47.20.−k, 03.40.Gc, 47.54.+r

I. INTRODUCTION

Fluid systems, especially Rayleigh-Bénard convection [1–4] served during the recent era of enormous progress in nonlinear science as variable and quantitative model systems for pattern formation, chaos, and turbulence [4–10]. Spatially extended experimental setups of high symmetry are often appropriate to address questions from those fields. A system of high symmetry is, for example, thermal convection in a two-dimensional extended fluid layer between ideally flat bottom and top container boundaries.

In actual fluid experiments effects of side walls and other symmetry breaking deformations or imperfections at container boundaries cannot be avoided in general. Related phenomena may be kept small under certain experimental conditions. However, during recent years the resolution in experiments has been enhanced dramatically and even the detection of thermal fluctuations became feasible in macroscopic pattern forming systems [11–14]. Therefore, it becomes increasingly likely that even small imperfections modify detected signals in an unexpected and puzzling way with such high experimental resolutions. One may be inclined to call such deviations from perfect geometries dirty effects. On the other hand, as discussed in this work, they also give rise to interesting new phenomena, which are not present in systems of high symmetry.

Side walls, for instance, lead to restrictions of the band of stable wave numbers for cellular patterns [15] or may select the orientation of convection rolls [16–19]. In traveling wave systems, such as thermal convection in fluid mixtures, they can trigger reflection effects and other dynamic phenomena [20–22] or they induce dynamic structures in rotating Rayleigh-Bénard convection [23–25]. Interesting nonlinear wave number selection processes [26–28] or even phase diffusion [28, 29] are triggered by reduced symmetries, namely, by a slow and/or a smooth (nonperiodic) variation of the thickness of the fluid layer and a smooth variation of the temperature difference across the fluid layer. A periodically varying thickness of the fluid layer, achieved by undulated top and bottom container boundaries and a phase shift between both, leads to a drifting cellular pattern as shown in a recent experiment [30]. The drift direction in this example depends on the relative phase between both periodic modulations.

Statistically distributed imperfections at container boundaries may lead to localized cellular structures at the threshold of thermal convection, similar to those already observed for gravity waves [31, 32]. Such localizations modify the bifurcation behavior of cellular structures in a characteristic manner, as shown for a model system [33]. Localized cellular patterns occur also in convection in porous media [34, 35].

Like finite size and disorder effects in phase transitions near thermal equilibrium it is also an important issue to understand how they affect pattern formation far from equilibrium. Natural phenomena occur in imperfect environments, thus the understanding of finite size and disorder effects on pattern formation may also help in interpreting correctly many phenomena such as geology or meteorology in terms of well defined laboratory systems.

To gain some theoretical insight about the effects of roughness in pattern formation it is often helpful to replace the roughness by periodic modulations. One may replace, for instance, imperfections at container boundaries in convection by temperature variations at the boundaries and undulations of the boundaries itself and analyze their consequences for the onset and nonlinear behavior of convection. There are a number of investigations about the effects of periodic temperature modulations [30, 36–38] and boundary undulations in Rayleigh-Bénard convection [30, 38–41]. An interesting case occurs when the wave number for the external modulation, q_M, is nearly commensurate to the critical wave number of the cellular pattern q_c: $q_M \sim 1,2,3,4 q_c$. For this case commensurable-incommensurable transitions in nonequilibrium systems occur as a function of the deviation from the commensurate ratios [42–47]. In quasi-two-dimensional convective systems a single periodic modulation of external parameters can lead to undulated or two-dimensional quasiperiodic patterns [48–50], which have some similarity to spontaneously occurring wave number competition in convection above secondary bifurcations [51].

These examples show that a number of interesting effects

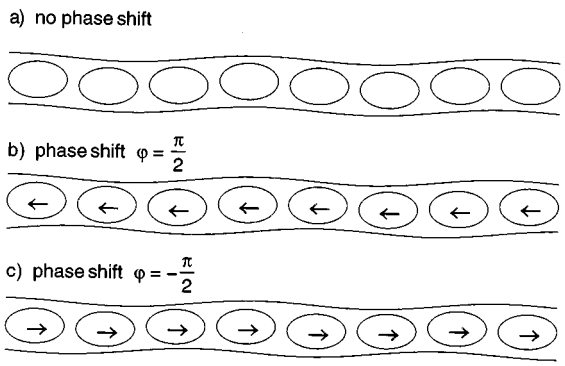

FIG. 1. A sketch of a Rayleigh-Bénard convection cell with wavy top and bottom boundaries. If the periodic undulations of the two boundaries are in phase, as shown in (a), then stationary convection rolls occur above threshold. A phase shift between the two boundary undulations, as indicated in (b) and (c), leads to drifting convection rolls above threshold and the drift direction depends on the sign of the relative phase φ.

in pattern formation are related to finite size or inhomogeneity effects. In this work we focus on a different type of periodic boundary modulation (as indicated below) being in some aspects closer to statistically distributed irregularities. We consider periodic temperature modulations at the top or bottom (or both) boundary of a cell for thermal convection combined with an undulation of one boundary.

For such a geometry we find a dynamic phenomenon, the so-call Hopf bifurcation by frustrated drifts. This effect is qualitatively described in Sec. I A and in more detail during the rest of the paper (see Secs. II–IV).

A. Qualitative description of the main result

It is well known that convection rolls occur in a horizontal layer heated from below. The difference, $\Delta T = T_l - T_u$, between the temperature at the bottom plate, T_l, and at the top plate, T_u, must increase beyond some threshold $\Delta T > \Delta T_c$ to induce convection [1–3].

When the top and the bottom boundaries in a Rayleigh-Bénard convection cell are plane and parallel, then below convection onset, $\Delta T < \Delta T_c$, heat is transported diffusively through the fluid layer and convectively beyond ΔT_c. In the presence of an undulated boundary there is already convective flow with a periodicity of the external spatial modulation for arbitrary values of temperature differences ΔT. This flow may be weak for small temperature differences $\Delta T \ll \Delta T_c$, however, it can be already considerable for $\Delta T \sim \Delta T_c$, depending on the modulation amplitude of the boundary. The presence of this *primary flow* has various consequences for the onset of the ''usual'' convection rolls, which we call *secondary flow*. Their wavelength is mainly determined by the mean distance between the top and bottom plates d and less by the external modulation. When the top and the bottom plates are undulated by the same wave number and both modulations are in phase, as indicated in Fig. 1(a), then the fluid layer thickness is everywhere the same and the onset of the secondary convection is still stationary. However, if there is a relative phase shift between both modulations, as indicated in Figs. 1(b) and 1(c), then the secondary flow (convection rolls) drifts [30]. The drift direction depends on the sign of the relative phase between the undulation of the top and bottom boundary whereas the velocity depends on the modulus of the phase shift and on the amplitude of the modulations.

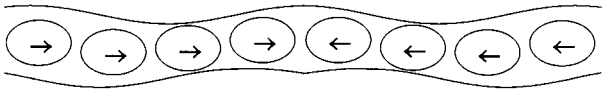

FIG. 2. A design of a convection cell is proposed that combines the geometry of Fig. 1(b) (right part) and of Fig. 1(c) (left part). The sign of the relative phase shift between the modulations of the top and bottom plates is reversed by a phase jump of the modulation on the bottom plate. The opposite sign in the left and right parts of the cell leads to virtually drifting convection rolls, which are frustrated. We will show that such frustrated drifts induced by periodically changing phase shifts lead to a new phenomenon: *Hopf bifurcation by frustrated drifts*.

For a finite phase shift between the boundary modulations, the thickness of the fluid layer is spatially varying and, as a consequence, the envelope of the secondary flow fields are spatially modulated, whereby the modulation wavelength is identical with the externally imposed wavelength.

Boundary modulations and their consequences are interesting by themselves, but they are also appropriate to model some aspects of heterogeneities occurring at the boundaries of the fluid container. Spatially homogeneous phase shifts between two periodic boundary modulations, such as in Fig. 1, are rather unlikely in real systems. A geometry as sketched in Fig. 2, where the relative phase changes periodically in space, seems more appropriate to mimic some aspects of statistically distributed imperfections at boundaries. Then the virtual drift directions alter periodically between neighboring phase jumps. Hence, the spatially averaged local drift direction would vanish, similar to that expected for randomly deformed top and bottom plates.

How might periodically reversed drift directions, corresponding to periodically repeated phase jumps such as in Fig. 2, affect the onset of the secondary flow? According to Figs. 1(b) and 1(c) one expects drifting secondary flow in every interval of homogeneous phase shift. However, since the virtual drifts have opposite drift direction in neighboring intervals, they may compensate each other and the secondary convection could be stationary and nondrifting. A further possibility seems imaginable. The secondary flow drifts in every interval of homogeneous phase shift and, in regions where the phase shift changes its sign, there might be a source or a sink for the drifting waves, depending on whether the drifts point to each other or from each other. We found a third possibility: these spatially varying virtual drift directions change the eigenvalue spectrum in such a way that above critical amplitudes of the boundary modulations the onset of convection is changed from a stationary into a oscillatory bifurcation. We call this phenomenon *Hopf bifurcation by frustrated drifts*. It has been recently predicted within a generalized Swift-Hohenberg equation [52] and the major task of this work is to discuss this phenomenon in terms of an experimentally accessible system, such as Rayleigh-Bénard convection.

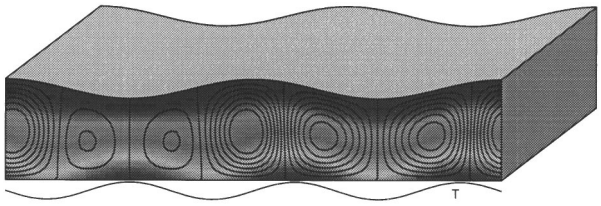

FIG. 3. An experimental design for a combination of an upper plate of corrugated form and a temperature modulation at the lower plate. The ratio of the wave numbers of the periodic undulation of the top plate (k_0) and the temperature modulation at the bottom plate (k_2) is $k_0:k_2=2:3$. The gray scale in the fluid layer indicates the temperature field of the primary flow and along the solid lines velocity potential of primary flow is constant. The curve below the cell indicates the temperature variation at the bottom plate.

To show by explicit calculations that this Hopf bifurcation by frustrated drifts occurs also for Rayleigh-Bénard convection, we actually replace in this work the ''didactic'' geometry with phase jumps in one boundary undulation, as shown in Fig. 2, by a smoother and essentially equivalent geometry of the convection cell. We choose a geometry as displayed in Fig. 3. For this convection cell the top boundary is undulated and the temperature at the bottom boundary is modulated, whereby the chosen wave numbers of both modulations have the ratio 2/3. Analytically, such a smooth geometry is much simpler to deal with and this choice of a cell design might have experimental advantages. It seems easier to change the amplitude of the temperature modulation by varying the local heating in an experiment. Changing the amplitude of boundary undulations would require several experiments with different cells of different modulation amplitudes for the boundary deformation. Nevertheless, we do need at least one boundary undulation to break the up-down symmetry, which is essential for the occurrence of the phenomenon Hopf bifurcation by frustrated drifts. With two temperature modulations only, this effect will be absent for Boussinesq fluids.

B. Description of the content

In Sec. II the basic equations for thermal convection are summarized and the boundary conditions as well as the boundary modulations are specified. In Sec. III we give analytical expressions for the basic flow under modulated conditions and we describe the linear stability analysis of the periodic basic flow in the limit of long wavelength modulations. In Sec. IV the numerical analysis of the equations as presented in Sec. III is given. The primary flow as well as the properties of the secondary flow at threshold are presented. With Sec. V we finish with a few concluding remarks. (A few selected aspects have been already described in two short communications [52, 53] and a more extended description of a part has been given in Ref. [54].)

II. BASIC EQUATIONS AND GEOMETRY

A. Basic equations

A simple fluid in a gravitational field under the action of an external temperature gradient is considered. Our investigations are restricted to a two-dimensional situation, with the vertical z coordinate and the horizontal x coordinate. The assumed incompressibility,

$$\partial_x v_x+\partial_z v_z=0, \tag{2.1}$$

allows one to define the two velocity components in terms of the scalar function Ψ:

$$v_x=\partial_z\Psi, \tag{2.2a}$$

$$v_z=-\partial_x\Psi. \tag{2.2b}$$

In the Boussinesq approximation, which is considered here, the equations of motion for the velocity potential $\Psi(\mathbf{r},t)$ and the temperature $T(\mathbf{r},t)$ of the fluid are [7, 55]

$$\partial_t\Delta\Psi=\nu\Delta^2\Psi-g\alpha\partial_x T-(\partial_z\Psi\partial_x-\partial_x\Psi\partial_z)\Delta\Psi, \tag{2.3a}$$

$$\partial_t T=\kappa\Delta T-(\partial_z\Psi\partial_x-\partial_x\Psi\partial_z)T. \tag{2.3b}$$

We scale all lengths in units of the thickness d, the velocities in units of κ/d, the temperature in units of $\kappa\nu/\alpha g d^3$ and the time in units of d^2/κ. Furthermore, we consider the limit of large Prandtl numbers $P=\nu/\kappa\gg 1$. The scaled versions of the equations of motions to be considered during this work are

$$0=\Delta^2\Psi-\partial_x T, \tag{2.4a}$$

$$\partial_t T=\Delta T+(\partial_x\Psi\partial_z-\partial_z\Psi\partial_x)T. \tag{2.4b}$$

B. Boundary conditions

Rigid as well as stress free boundary conditions for the velocity are considered, however, with periodic modulations of the temperature at the top and bottom plates as well as a periodic undulated top plate. The bottom plate is located at $z=0$ and the top plate at

$$z=1+H_0(x)$$

with

$$H_0(x)=F_0\cos(k_0 x) \quad \text{and} \quad k_0=n_0 k. \tag{2.5}$$

Ideal conductivity of the bounding plates is assumed, which leads to the following boundary conditions for the temperature field:

$$T(x,z)=T_u+H_1(x) \quad \text{at} \quad z=1+H_0(x), \tag{2.6a}$$

$$T(x,z)=T_l+H_2(x) \quad \text{at} \quad z=0, \tag{2.6b}$$

with modulations

$$H_1(x)=F_1\cos(k_1 x+\varphi_1) \quad (k_1=n_1 k), \tag{2.7a}$$

$$H_2(x)=F_2\cos(k_2 x+\varphi_2) \quad (k_2=n_2 k). \tag{2.7b}$$

Only integer values for n_i are considered and therefore only commensurate ratios between the modulation wave numbers are allowed. For both the stress-free as well as the rigid-boundary conditions, the boundaries are impenetrable and therefore the vertical component of the velocity $v_z=-\partial_x\Psi$ has to vanish at the boundaries:

$$\Psi(x,z)=0 \quad \text{at} \quad z=0,1+H_0(x). \tag{2.8}$$

For rigid (realistic) boundary conditions also the horizontal velocity parallel to the surface $v_{\parallel}=(\mathbf{n}\cdot\nabla)\Psi$ must vanish:

$$(\mathbf{n}\cdot\nabla)\Psi(x,z)=0 \quad \text{at} \quad z=0,1+H_0(x). \tag{2.9}$$

n is the vector normal to the boundary. For stress-free boundary conditions the first derivative of the velocity parallel to the boundary has to vanish:

$$(\mathbf{n}\cdot\nabla^2)\Psi(x,z)=0 \quad \text{at} \quad z=0,1+H_0(x). \tag{2.10}$$

With the above definitions of the boundary conditions and the introduced temperature scaling the well-known Rayleigh number is now proportional to the mean temperature difference between the top and bottom plates:

$$R=T_l-T_u=\frac{\alpha g d^3 \Delta T}{\nu\kappa}. \tag{2.11}$$

III. METHODS OF SOLUTION: BASIC STATE, LINEAR STABILITY, AMPLITUDE EQUATIONS

The modulation wavelength λ_M is taken much bigger than the thickness of the fluid layer, $\lambda_M \gg d$, for advantages explained in the following.

Without modulations at the boundaries, the primary state has a linear temperature profile interpolating between the top and bottom temperature, and there is no convective fluid motion. The undulations of the bounding plates or the modulations of the temperature at the boundaries induce a primary convective flow for arbitrary values of the mean temperature difference, T_l-T_u. This primary flow and the temperature field have the periodicity of the external modulations.

In the absence of modulations and for R above the critical value R_c the linear temperature profile (primary state) becomes unstable against convection rolls (secondary state) with a wavelength of the order of the layer thickness, $\lambda_c \sim d$ [3, 56]. For modulation wavelengths much larger than the thickness of the fluid layer one has a clear separation of the length scales of the primary and secondary fields of the temperature and flow. Hence, a sharp threshold for the onset of the secondary flow can be expected as in the unmodulated case. Therefore, it is reasonable to divide the whole solution into the long wavelength or homogeneous primary fields, $\overline{\Psi}(x,z)$, $\overline{T}(x,z)$, and into the short wavelength secondary fields, $\Phi(x,z,t)$, $\Theta(x,z,t)$:

$$\Psi(x,z,t)=\overline{\Psi}(x,z)+\Phi(x,z,t), \tag{3.1a}$$

$$T(x,z,t)=\underbrace{\overline{T}(x,z)}_{\text{primary}}+\underbrace{\Theta(x,z,t)}_{\text{secondary}}. \tag{3.1b}$$

Symbolically, the equations of motion given in Eq. (2.4) can be written as

$$\mathscr{M}\partial_t\vec{u}=\mathscr{L}\vec{u}+\vec{N}(\vec{u},\vec{u}), \tag{3.2}$$

with

$$\vec{u}=\begin{pmatrix}\Psi\\ T\end{pmatrix}, \quad \vec{u}=\vec{u}_1+\vec{u}_2=\begin{pmatrix}\overline{\Psi}\\ \overline{T}\end{pmatrix}+\begin{pmatrix}\Phi\\ \Theta\end{pmatrix}. \tag{3.3}$$

$\mathscr{M}$ and $\mathscr{L}$ are linear operators and $\vec{N}(,)$ describes the nonlinear parts of Eqs. (2.4).

With rather different length scales of the primary and secondary convective states, the equations of motion for $\vec{u}_1$ and $\vec{u}_2$ can be separated and formulated in the following form:

$$\mathscr{M}\partial_t\vec{u}_1=\mathscr{L}\vec{u}_1+\vec{N}(\vec{u}_1,\vec{u}_1), \tag{3.4}$$

$$\mathscr{M}\partial_t\vec{u}_2=\mathscr{L}_2\vec{u}_2+\vec{N}(\vec{u}_2,\vec{u}_2). \tag{3.5}$$

The linear operator in the latter equation, $\mathscr{L}_2$, depends on the primary state. As indicated above, the linear part of Eq. (3.5) provides in this limit a well-defined threshold for the onset of the secondary flow $\vec{u}_2$. [Without that separation of the length scales the bifurcation into the secondary state would be imperfect and the separation into the two equations of motion (3.4), (3.5) is not reasonable.]

The long wavelength modulation ($kd \ll 1$) has in addition to the ''sharp'' threshold the conceptual advantage that $kd \ll 1$ can be taken as a small ''expansion'' parameter. Especially for undulated boundaries, this small parameter allows within a perturbation expansion the transformation into coordinate systems with flat boundaries, where the equations of motion are still of reasonable extent (see Sec. III B 1). Also the primary state can be calculated analytically for the leading order of k. Both aspects reduce considerably the technical effort for calculations with modulated geometries.

In this section first the primary flow is determined essentially analytically from Eq. (3.4): In Sec. III A 1 for a single temperature modulation and in Sec. III B 2 for a wavy top boundary with simultaneous temperature modulations on both boundaries. At the second step in Secs. III A 2 and III B 3 the equations for the stability properties of the primary state, namely, the explicit form of the linear part of Eq. (3.5) and its solutions are formulated. The numerical analysis of these linear equations is given in Sec. IV.

A. Temperature modulation at the bottom plate

First we describe the effects for the onset of convection as they are induced by only one spatially periodic temperature modulation, for example, at the bottom plate ($H_0=H_1=0$). That is a simple enough configuration to demonstrate explicitly the calculational scheme for stress-free boundary conditions (2.8) and (2.10). In the next subsection (III B), where we consider the temperature modulation at the top or at the bottom plate simultaneously with the undulation of the top plate, we can no longer show all the steps of the analysis explicitly in the available, limited space.

1. The primary flow

Since we are restricting ourselves to long wavelength modulations $kd \ll 1$, we can employ a perturbational ansatz for the primary state:

$$\overline{T}(x,z)=\overline{T^0}(x,z)+k\overline{T^1}(x,z)+O(k^2), \tag{3.6a}$$

$$\overline{\Psi}(x,z)=\overline{\Psi^0}(x,z)+k\overline{\Psi^1}(x,z)+O(k^2). \tag{3.6b}$$

These fields must fit the periodicity of the temperature modulation at the boundary and can be expanded into Fourier

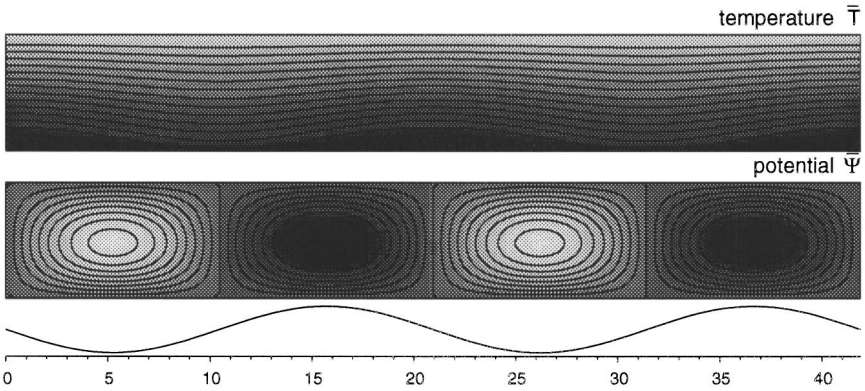

FIG. 4. The primary flow for the spatially modulated temperature at the bottom plate is shown [as given analytically in Eq. (3.15)]. The temperature field $\overline{T}$ is shown in the top part and the potential $\overline{\Psi}$ in the middle. The Rayleigh number was taken at the threshold of the secondary flow, with the modulation amplitude $F_2=0.1R_c^f$ and wave number $k_2=0.3$. The lower part shows the x dependence of the potential $\overline{\Psi}$ at $z=1/2$. (The dark areas correspond to larger values for the fields Ψ and T and the bright areas to smaller values for both fields.)

series. Setting the Fourier ansatz into Eqs. (2.4) and using the fact that the derivatives ∂_x^n are of the order $O(k^n)$, we end up with the following hierarchy of equations. At the order $O(k^0)$ we have

$$\partial_z^4\overline{\psi^0}=0, \tag{3.7a}$$

$$\partial_z^2\overline{T^0}=0, \tag{3.7b}$$

and at order $O(k^1)$,

$$\partial_z^4\overline{\Psi^1}(x,z)=\frac{\partial_x\overline{T^0}}{k}, \tag{3.8a}$$

$$\partial_z^2\overline{T^1}(x,z)=\frac{1}{k}(\partial_z\overline{\Psi^0}\partial_x\overline{T^0}-\partial_z\overline{T^0}\partial_x\overline{\Psi^0}). \tag{3.8b}$$

Equation (3.7b) can be solved by a polynomial ansatz:

$$\overline{T^0}(z)=c_1+c_2z. \tag{3.9}$$

From the boundary conditions, $\overline{T^0}(x,z=0)=T_l+H_2(x)$ and $\overline{T^0}(x,z=1)=T_u$, we can determine the coefficients c_1 and c_2 and obtain the final expression for the temperature field,

$$\overline{T^0}(z)=T_l+H_2(x)-z(R+H_2(x)), \tag{3.10}$$

with $R=T_l-T_u$. According to homogeneous boundary conditions for the velocity potential Ψ^0 is independent of x. Hence, also Eq. (3.7a) can be solved with the polynomial ansatz

$$\overline{\Psi^0}(x,z)=c_1+c_2z+c_3z^2+c_4z^3. \tag{3.11}$$

For the assumed stress-free boundary conditions all the coefficients $c_i=0$ vanish and therefore the velocity potential does as well: $\overline{\Psi^0}(x,z)=0$.

Using again a polynomial ansatz with respect to z, it is easy to show that the temperature field vanishes at first order in k: $\overline{T^1}(x,z)=0$. With its explicit form of $\overline{T^0}(z)$ as given in Eq. (3.10), Eq. (3.8a) takes the form

$$\partial_z^4\overline{\Psi^1}=(z-1)\partial_xH_2(x)/k, \tag{3.12}$$

which is solved by

$$\overline{\Psi^1}(x,z)=P(z)\partial_xH_2(x)/k, \tag{3.13}$$

wherein the polynomial $P(z)$ is defined as

$$P(z)=\frac{1}{360}(-8z+20z^3-15z^4+3z^5). \tag{3.14}$$

In leading order of the k expansion the primary flow is

$$\overline{\Psi}(x,z)=-P(z)\partial_xH_2(x)+O(k^3), \tag{3.15a}$$

$$\overline{T}(x,z)=T_l+H_2(x)-z(R+H_2(x))+O(k^2). \tag{3.15b}$$

In the next paragraph we will show that this primary state leads to a modified onset of the Rayleigh-Bénard convection rolls. (The form of the primary flow is depicted in Fig. 4.)

2. Linear stability of the primary flow

Equations (3.5), linear in Θ and Φ, take with the primary flow given in Eqs. (3.15) the form

$$0=\partial_x\Theta-\Delta^2\Phi, \tag{3.16a}$$

$$\partial_t\Theta=\Delta\Theta-\partial_z\overline{\Psi}\partial_x\Theta+(\partial_z\overline{T}\partial_x-\partial_x\overline{T}\partial_z)\Phi. \tag{3.16b}$$

A parameter set can be calculated at which the primary flow becomes unstable against the small inhomogeneous perturbations Φ and Θ. By eliminating the temperature field Θ, the analysis of the above equations can be simplified further. For that we differentiate Eq. (3.16b) with respect to x and eliminate Θ from Eq. (3.16a). The resulting linear equation in Φ may be solved with the separation ansatz

$$\Phi(x,z,t)=\Phi_1(x)\Phi_2(z)e^{\sigma t}. \tag{3.17}$$

For the homogeneous stress-free boundary conditions $\Phi_2(z)=\sin(\pi z)$ is an exact solution. To approximate the exact z dependence in the presence of the spatially modulated

temperature one has to use the series $\Phi_2(z) = \sum_{m=1}^{N} \sin(m\pi z)$ up to some appropriate number N. Here, we keep only the first member of this series, $\sin(\pi z)$ $(N=1)$. This simplifies the analysis in the following considerably; however, it keeps the essential effects. To remove the explicit z dependence in Eqs. (3.16), we multiply the equations from the left by $\sin(\pi z)$ and integrate with respect to z. Then the equation linear in Φ_1 is obtained up to $O(k)$:

$$\sigma(\partial_x^2-\pi^2)^2\Phi_1=(\partial_x^2-\pi^2)^3\Phi_1 - \frac{1}{16\pi^4}(\partial_x^2-\pi^2)^2\partial_x H_2(x)\partial_x\Phi_1 - \frac{3}{2}\partial_x H_2(x)\partial_x\Phi_1-[R+H_2(x)]\partial_x^2\Phi_1. \tag{3.18}$$

This linear ordinary differential equation is solved by a Floquet ansatz

$$\Phi_1(x)=e^{iqx}\sum_{l=-N}^{N} g_l e^{ilkx}. \tag{3.19}$$

Without thermal modulation $(H_2=0)$ all coefficients besides g_0 vanish. Sorting all the terms proportional to e^{ilkx} we end up with the eigenvalue problem,

$$\sigma\vec{g}=\mathscr{A}\vec{g} \quad [\vec{g}=(g_{-N},\ldots,g_N)], \tag{3.20}$$

where the matrix $\mathscr{A}$ is a band matrix of width $(2n_2+1)$:

$$\mathscr{A}_{l,l}=-(\alpha^2+\pi^2)+R\frac{\alpha^2}{(\alpha^2+\pi^2)^2}, \tag{3.21a}$$

$$\mathscr{A}_{l,l-n_2}=\frac{1}{2}F_2\frac{1}{(\alpha^2+\pi^2)^2}\beta\left(\beta+k\frac{1}{16\pi^4}(\beta^2+\pi^2)^2+\frac{3}{2}k\right), \tag{3.21b}$$

$$\mathscr{A}_{l,l+n_2}=\frac{1}{2}F_2\frac{1}{(\alpha^2+\pi^2)^2}\gamma\left(\gamma-k\frac{1}{16\pi^4}(\gamma^2+\pi^2)^2-\frac{3}{2}k\right). \tag{3.21c}$$

F_2 is the amplitude of the temperature modulation and the constants are defined as follows:

$$\alpha=q+kl, \tag{3.22a}$$

$$\beta=q+k(l-n_2), \tag{3.22b}$$

$$\gamma=q+k(l+n_2). \tag{3.22c}$$

From the solvability condition for the homogeneous system of equations (3.20),

$$\det(\sigma\mathscr{T}-\mathscr{A})=f(\sigma,q^2,R,F_2,k^2,\ldots), \tag{3.23}$$

the eigenvalues σ_i are determined as a function of the parameters ($\mathscr{T}$ is the unity matrix). We sort the spectrum σ_i in ascending order with respect to the real parts and calculate the eigenvalue with the largest real part:

$$\sigma=\max[\mathrm{Re}(\sigma_i)]. \tag{3.24}$$

The linear perturbations Θ and Φ with respect to the primary flow grow for the chosen parameter combinations if $\sigma>0$ and they decay if $\sigma<0$. We are interested in the neutrally stable case $\sigma=0$, separating the stable from the unstable regime. Keeping all parameters beside q fixed, the condition $\sigma=0$ gives via Eq. (3.23) an implicit condition for the determination of the Rayleigh number $R_0(q^2,\ldots)$ at the instability point. $R_0(q)$ is the so-called *neutral curve*. For of a *Hopf bifurcation* one has a degenerated complex conjugate pair,

$$\sigma=\lambda\pm i\omega, \tag{3.25}$$

with the Hopf frequency ω as the imaginary part. The onset of convection happens above the minimum of the neutral curve $R_0(q)$, $R_c=\min[R_0(q)]=R_0(q=q_c)$. In case of a Hopf bifurcation we call the frequency at that point the critical frequency: $\omega_c=\omega_0(q=q_c)$. For $H_2=0$ we recover the well-known threshold for stress-free boundary conditions and unmodulated temperature,

$$R_0(q)=\pi^4\frac{(\pi^2+q^2)^3}{q^2}, \tag{3.26}$$

with the critical values $R_0(q=q_c)=R_c=27\pi^4/4=657.6$, $q_c=\pi/\sqrt{2}=2.221$, and $\omega_c=0$.

B. Wavy boundary plus temperature modulation

Here we proceed to the more general boundary modulations. The primary flow as well as its stability properties are calculated in the presence of a wavy top boundary plate and simultaneous modulations of the temperature field at the top and the bottom plates as introduced in Sec. II B. The scheme explained in the next subsections is described for rather general combinations of temperature modulations H_1, H_2 and boundary undulation H_0. Nevertheless we will concentrate in Sec. IV mainly on the following cases: (i) Geometric undulation of the top boundary $n_0=1$, $H_1(x)=0$, $H_2(x)=0$; (ii) two temperature modulations with wave number ratios $k_1:k_2=1:1$ and $2:3$; (a) $n_1=1$, $n_2=1$, $H_0(x)=0$, (b) $n_1=2$, $n_2=3$, $H_0(x)=0$; (iii) upper wavy boundary and temperature modulation at the bottom boundary with wave number ratios $k_0:k_2=1:1$ and $2:3$; (a) $n_0=1$, $n_2=1$, $H_1(x)=0$, (b) $n_0=2$, $n_2=3$, $H_1(x)=0$.

1. Transformation into flat boundaries

To calculate the primary flow as well as its stability properties in the presence of a boundary undulation it is convenient to transform into a coordinate system where the boundaries become flat again. The transformation to the new coordinates ξ and η is as follows (see [39]):

$$\xi=x, \quad \eta=\frac{z}{1+H_0(x)}. \tag{3.27}$$

Within this definition the bottom and top boundaries are located at $\eta=0,1$. After the transformation of the equations of motion (2.4) into the new coordinates we keep terms up to the leading order in the modulation wave number k. Otherwise the differential operators become rather cumbersome. The details of the operator transformation are given in the

Appendix and the equations of motion in the transformed system are, up the leading order in k,

$$(\partial_\xi+\eta B\partial_\eta)T=(\partial_\xi^4+A^4\partial_\eta^4+4\eta B\partial_\xi^3\partial_\eta+2A^2\partial_\xi^2\partial_\eta^2 +8A^2B\partial_\xi\partial_\eta^2+4A^2B\eta\partial_\xi\partial_\eta^3)\Psi, \tag{3.28a}$$

$$\partial_t T=-A\partial_\eta\Psi(\partial_\xi+\eta B\partial_\eta)T+(\partial_\xi+\eta B\partial_\eta)\Psi A\partial_\eta T +(\partial_\xi^2+A^2\partial_\eta^2+2\eta B\partial_\xi\partial_\eta)T, \tag{3.28b}$$

with

$$A(\xi)=\frac{1}{1+H_0(\xi)}=\frac{1}{1+F_0\cos(k_0\xi)}, \tag{3.29a}$$

$$B(\xi)=\frac{-\partial_\xi H_0(\xi)}{1+H_0(\xi)}=\frac{k_0F_0\sin(k_0\xi)}{1+F_0\cos(k_0\xi)}. \tag{3.29b}$$

The conditions for stress-free boundaries described in Sec. II B are in the transformed coordinate system:

$$T(\xi,\eta=0)=T_l+H_2(\xi), \tag{3.30a}$$

$$T(\xi,\eta=1)=T_u+H_1(\xi), \tag{3.30b}$$

$$\Psi(\xi,\eta=0,1)=0, \tag{3.30c}$$

$$\partial_\eta^2\Psi(\xi,\eta=0,1)=0. \tag{3.30d}$$

For rigid boundary conditions the latter condition (3.30d) is changed into

$$\partial_\eta\Psi(\xi,\eta=0,1)=0. \tag{3.31}$$

2. The primary flow

We use again the expansion given in Eqs. (3.6) for the calculation of the primary flow from Eqs. (3.28). The equations for the fields in leading order, $\overline{\Psi^0},\overline{T^0}\propto O(k^0)$, are

$$A^4\partial_\eta^4\overline{\Psi^0}(\xi,\eta)=0, \tag{3.32}$$

$$A^2\partial_\eta^2\overline{T^0}(\xi,\eta)=0. \tag{3.33}$$

$\overline{\Psi^0}(\xi,\eta)=0$ vanishes again and with the polynomial ansatz $\overline{T^0}(\xi,\eta)=c_1+c_2\eta$ we find from Eq. (3.33),

$$\overline{T^0}(\xi,\eta)=T_l+H_2(\xi)+\eta(H_1(\xi)-H_2(\xi)-R). \tag{3.34}$$

The equations for the fields in next higher order $O(k^1)$ read

$$A^4\partial_\eta^4\overline{\Psi^1}(\xi,\eta)=\frac{1}{k}(\partial_\xi+\eta B\partial_\eta)\overline{T^0}, \tag{3.35}$$

$$A^2\partial_\eta^2\overline{T^1}(\xi,\eta)=0. \tag{3.36}$$

From Eq. (3.36) one finds again $\overline{T^1}=0$ and with the explicit form of T^0 Eq. (3.35) takes the form

$$kA^4\partial_\eta^4\overline{\Psi^1}=M_1(\xi)+\eta M_2(\xi), \tag{3.37}$$

with

$$M_1=\partial_\xi H_2(\xi), \tag{3.38}$$

$$M_2=\partial_\xi(H_1(\xi)-H_2(\xi))+B(\xi)(H_1(\xi)-H_2(\xi)-R). \tag{3.39}$$

Using a polynomial ansatz for this ordinary differential equation the primary flow up to $O(k)$ is given by

$$\overline{\Psi}(\xi,\eta)=\frac{k}{A^4}[P_1(\eta)M_1(\xi)+P_2(\eta)M_2(\xi)], \tag{3.40}$$

$$\overline{T}(\xi,\eta)=T_l+H_2(\xi)+\eta(H_1(\xi)-H_2(\xi)-R), \tag{3.41}$$

with

$$P_1(\eta)=\frac{1}{360}(15\eta-30\eta^3+15\eta^4), \tag{3.42a}$$

$$P_2(\eta)=\frac{1}{360}(7\eta-10\eta^3+3\eta^5) \tag{3.42b}$$

for stress-free boundaries and

$$P_1(\eta)=\frac{1}{120}(5\eta^2-10\eta^3+5\eta^4), \tag{3.43a}$$

$$P_2(\eta)=\frac{1}{120}(2\eta^2-3\eta^3+\eta^5) \tag{3.43b}$$

for rigid boundary conditions.

3. Linear stability of the primary flow

The separation ansatz given in Eqs. (3.1) together with the transformed equations of motion (3.28) lead to two coupled linear equations for the fields Φ and Θ with periodic coefficients:

$$\left(\frac{1}{A^4}\partial_\xi+\eta\frac{B}{A^4}\partial_\eta\right)\Theta=\left(\frac{1}{A^4}\partial_\xi^4+\partial_\eta^4+4\eta\frac{B}{A^4}\partial_\xi^3\partial_\eta+2\frac{1}{A^2}\partial_\xi^2\partial_\eta^2 +8\frac{B}{A^2}\partial_\xi\partial_\eta^2+4\frac{B}{A^2}\eta\partial_\xi\partial_\eta^3\right)\Phi, \tag{3.44}$$

$$\frac{1}{A^2}\partial_t\Theta=-\frac{1}{A}\partial_\eta\overline{\Psi}\partial_\xi\Theta-\frac{1}{A}\partial_\eta\Phi\partial_\xi\overline{T}+\frac{1}{A}\partial_\eta\overline{T}\partial_\xi\Phi +\left(\frac{1}{A^2}\partial_\xi^2+\partial_\eta^2+2\frac{B}{A^2}\eta\partial_\xi\partial_\eta\right)\Theta. \tag{3.45}$$

The periodic coefficients have the periodicity of the boundary modulations and the ξ and η dependence can be separated with the following Floquet-type ansatz:

$$\Phi(\xi,\eta,t)=e^{\sigma t+iq\xi}\sum_{l=-N,m=1}^{N,M_P}e^{ilk\xi}f_m(\eta)+\text{c.c.}, \tag{3.46}$$

$$\Theta(\xi,\eta,t)=e^{\sigma t+iq\xi}\sum_{l=-N,m=1}^{N,M_P} T_{l,m}e^{ilk\xi}\sin(m\pi\eta)+\text{c.c.}, \tag{3.47}$$

(c.c. denotes the complex conjugate). For free boundary conditions $f_m(\eta)$ is of the form

$$f_m(\eta)=\sin(m\pi\eta), \tag{3.48}$$

and for rigid ones $f_m(\eta)$ can be expressed for even and odd values of m in terms of Chandrasekhar functions C_m and S_m [3]

$$f_m(\eta)=C_m(\eta) \quad (\text{for } m \text{ even}), \tag{3.49a}$$

$$f_m(\eta)=S_m(\eta) \quad (\text{for } m \text{ odd}), \tag{3.49b}$$

which are defined by the following expressions:

$$C_m(\eta)=\frac{\cosh\left[\lambda_m\left(\eta-\frac{1}{2}\right)\right]}{\cosh\left(\frac{1}{2}\lambda_m\right)}-\frac{\cos\left[\lambda_m\left(\eta-\frac{1}{2}\right)\right]}{\cos\left(\frac{1}{2}\lambda_m\right)}, \tag{3.50}$$

$$S_m(\eta)=\frac{\sinh\left[\mu_m\left(\eta-\frac{1}{2}\right)\right]}{\sinh\left[\frac{1}{2}\mu_m\right]}-\frac{\sin\left[\mu_m\left(\eta-\frac{1}{2}\right)\right]}{\sin\left(\frac{1}{2}\mu_m\right)}. \tag{3.51}$$

Herein λ_m and μ_m are solutions of the following two equations:

$$\tanh(\tfrac{1}{2}\lambda_m)+\tan(\tfrac{1}{2}\lambda_m)=0, \tag{3.52}$$

$$\coth(\tfrac{1}{2}\mu_m)+\cot(\tfrac{1}{2}\mu_m)=0\,. \tag{3.53}$$

To transfer the linear equations into an eigenvalue problem for the constant coefficients $T_{l,m}$ and $P_{l,m}$ one has to eliminate the remaining dependence on ξ and η by projecting Eq. (3.45) onto

$$\int_{-\infty}^{\infty}d\xi\int_0^1 d\eta e^{-ikl}f_n(\eta)\odot \tag{3.54}$$

and Eq. (3.44) onto

$$\int_{-\infty}^{\infty}d\xi\int_0^1 d\eta e^{-ikl}\sin(n\pi\eta)\odot. \tag{3.55}$$

This leads to two coupled linear equations:

$$i\mathscr{A}_1\vec{\Theta}=\mathscr{A}_2\vec{\Phi}, \tag{3.56}$$

$$\sigma\mathscr{B}_1\vec{\Theta}=\mathscr{B}_2\vec{\Theta}+i\mathscr{B}_3\vec{\Phi}, \tag{3.57}$$

where the vectors $\vec{\Theta}$ and $\vec{\Phi}$ are defined by

$$\vec{\Phi}=\begin{pmatrix}\vec{\Phi}^1\\ \vdots\\ \vec{\Phi}^{M_P}\end{pmatrix} \quad \text{and} \quad \vec{\Theta}=\begin{pmatrix}\vec{\Theta}^1\\ \vdots\\ \vec{\Theta}^{M_T}\end{pmatrix} \tag{3.58}$$

and the subvectors by

$$\vec{\Phi}^m=\begin{pmatrix}P_{m,N}\\ \vdots\\ P_{m,-N}\end{pmatrix} \quad \text{and} \quad \vec{\Theta}^m=\begin{pmatrix}T_{m,N}\\ \vdots\\ T_{m,-N}\end{pmatrix}. \tag{3.59}$$

The matrices $\mathscr{A}_1$ and $\mathscr{A}_2$ are of a block structure:

$$\mathscr{A}_i=\begin{pmatrix}\mathscr{A}_i^{11} & \cdots & \mathscr{A}_i^{M_P1}\\ \vdots & & \vdots\\ \mathscr{A}_i^{1M_T} & \cdots & \mathscr{A}_i^{M_PM_T}\end{pmatrix}. \tag{3.60}$$

The matrices $\mathscr{B}_1$, $\mathscr{B}_2$, and $\mathscr{B}_3$ are of a similar form; however, the dimensions M_T and M_P are exchanged.

The submatrices are of the dimension $(2N+1)\times(2N+1)$, with a bandwidth up to $n_0\max(n_1,n_2)$. They can be written in terms of the vector

$$\vec{E}(\xi)=(e^{-iNk\xi},\ldots,e^{iNk\xi}), \tag{3.61}$$

with the help of the dyadic product $\odot$ and the abbreviation

$$\langle U\rangle=\int_{-\infty}^{\infty}d\xi\int_0^1 d\eta U(\xi,\eta) \tag{3.62}$$

in the following form:

$$\mathscr{A}_1^{mn}=\langle\vec{E}^*(\xi)\odot f_m(\eta)a_1\sin(n\pi\eta)\vec{E}(\xi)\rangle, \tag{3.63a}$$

$$\mathscr{A}_2^{mn}=\langle\vec{E}^*(\xi)\odot f_m(\eta)a_2 f_n(\eta)\vec{E}(\xi)\rangle, \tag{3.63b}$$

$$\mathscr{B}_1^{mn}=\langle\vec{E}^*(\xi)\odot\sin(m\pi\eta)b_1\sin(n\pi\eta)\vec{E}(\xi)\rangle, \tag{3.63c}$$

$$\mathscr{B}_2^{mn}=\langle\vec{E}^*(\xi)\odot\sin(m\pi\eta)b_2\sin(n\pi\eta)\vec{E}(\xi)\rangle, \tag{3.63d}$$

$$\mathscr{B}_3^{mn}=\langle\vec{E}^*(\xi)\odot\sin(m\pi\eta)b_3 f_n(\eta)\vec{E}(\xi)\rangle. \tag{3.63e}$$

Herein the operators a_i and b_i are defined by

$$a_1=\frac{1}{A^4}\partial_\xi+\eta\frac{B}{A^4}\partial_\eta\,, \tag{3.64a}$$

$$a_2=\frac{1}{A^4}\partial_\xi^4+\partial_\eta^4+4\eta\frac{B}{A^4}\partial_\xi^3\partial_\eta+2\frac{1}{A^2}\partial_\xi^2\partial_\eta^2+8\frac{B}{A^2}\partial_\xi\partial_\eta^2 +4\frac{B}{A^2}\eta\partial_\xi\partial_\eta^3, \tag{3.64b}$$

$$b_1=\frac{1}{A^2}, \tag{3.64c}$$

$$b_2=-\frac{1}{A^5}(\partial_\eta P_1 M_1+\partial_\eta P_2 M_2)\partial_\xi+\frac{1}{A^2}\partial_\xi^2+\partial_\eta^2 +2\frac{B}{A^2}\eta\partial_\xi\partial_\eta, \tag{3.64d}$$

$$b_3=-\frac{1}{A}[\eta\partial_\xi(H_1-H_2)+\partial_\xi H_2]\partial_\eta+\frac{1}{A}(-R+H_1-H_2)\partial_\xi. \tag{3.64e}$$

The calculation of the submatrices $\mathscr{A}_i^{mn}$ is rather complex. Therefore we developed for the derivation of those an algorithm with the algebraic manipulation package MAPLE providing the Fortran source codes. This is especially helpful when we use different combinations of the external modulations.

Φ can be eliminated from Eq. (3.57) via

$$\vec{\Phi}=i.\mathscr{A}_2^{-1}.\mathscr{A}_1\vec{\Theta} \tag{3.65}$$

and one obtains the following eigenvalue equation:

$$\sigma.\mathscr{B}_1\vec{\Theta}=\mathscr{B}_2\vec{\Theta}-\mathscr{B}_3.\mathscr{A}_2^{-1}.\mathscr{A}_1\vec{\Theta}. \tag{3.66}$$

This can be formally simplified into

$$\sigma\vec{\Theta}=\mathscr{C}\vec{\Theta}, \tag{3.67}$$

with

$$\mathscr{C}=\mathscr{B}_1^{-1}(.\mathscr{B}_2-.\mathscr{B}_3.\mathscr{A}_2^{-1}.\mathscr{A}_1). \tag{3.68}$$

From the eigenvalue with the largest real part, $\lambda=\max[\mathrm{Re}(\sigma_i)]$, the neutral curve $R_0(q)$ and the Hopf frequency $\omega_0(q)$ can be determined via the condition $\lambda=0$. Minimizing $R_0(q)$ then gives again the critical Rayleigh number R_c, the critical wave number q_c, and in case of a Hopf bifurcation also the critical Hopf frequency ω_c.

The dependence of these critical quantities on the parameters is described in Sec. IV, whereby for all calculations the first three Chandrasekhar functions have been used. Using in the expansions (3.46) and (3.47) a larger number of these functions changes the results only slightly (quantitatively, not qualitatively). The convergence of the expansion has always been tested numerically. In addition the first six modes in the Floquet expansion (3.46) have been used, which are also a reasonable approximation.

C. Amplitude equations: Linear parts

In contrast to unmodulated Rayleigh-Bénard convection the eigenvalue spectrum of Eq. (3.67) contains under certain conditions also conjugate complex pairs with imaginary parts $\pm\omega$ (see Sec. IV C below). Those pairs become critical $[\mathrm{Re}(\sigma)=0, \mathrm{Im}(\sigma)=\pm\omega]$ at certain values for the amplitudes of the boundary undulation and the simultaneous temperature modulation and all other eigenvalues are still damped $\mathrm{Re}(\sigma)<0$. In such a case immediately above threshold the secondary flow is expected to be a traveling or a standing wave of the following form:

$$\Phi(\xi,\eta,t)=A_0 e^{i(q_c\xi+\omega_c t)}F^+(\xi,\eta)+B_0 e^{i(q_c\xi-\omega_c t)}F^-(\xi,\eta) +\text{c.c.} \tag{3.69}$$

$F^{+/-}$ correspond to the respective Hopf frequency $\pm\omega_c$ and is defined by the series [see also Eqs. (3.46) and 3.47)]:

$$F^{+/-}(\xi,\eta)=\sum_{l=-N}^{N}\sum_{m=1}^{M_P}P_{l,m}^{+/-}e^{ilk\xi}f_m(\eta). \tag{3.70}$$

Both functions have the periodicity $2\pi/k$ and describe in Eq. (3.69) a slow modulation of the fast varying traveling and standing wave part, $e^{i(\pm q_c x\pm w_c t)}$. For the temperature field $\Theta(\xi,\eta,t)$ a similar expression can be obtained; however, the amplitudes $P_{l,m}$ must be replaced by $T_{l,m}$.

For $B_0=0$ the expression in Eq. (3.69) describes a left traveling wave and for $A_0=0$ a right traveling wave. [For $\omega_c=0$ and $A_0=0$ or $B_0=0$ formula (3.69) describes a stationary quasiperiodic cellular structure.] Assuming nonconstant amplitudes A_0 and B_0, which are slowly varying on the spatial scales $2\pi/q_c$ and $2\pi/k$ as well as on the temporal scale $2\pi/\omega_c$, then one can derive for them envelope equations [57, 58] in a small ε neighborhood of the critical Rayleigh number R_c, with

$$\varepsilon=(R-R_c)/R_c. \tag{3.71}$$

The linear parts of such equations are well known and have the following form [59–61]:

$$\tau_0(\partial_t-v_g\partial_x)A_0=(\varepsilon+\delta\varepsilon)(1+ic_0)A_0+\xi_0^2(1+ic_1)\partial_x^2A_0 +(\text{nonlinear terms}), \tag{3.72a}$$

$$\tau_0(\partial_t+v_g\partial_x)B_0=\varepsilon(1+ic_0)B_0+\xi_0^2(1+ic_1)\partial_x^2B_0 +(\text{nonlinear terms}). \tag{3.72b}$$

$\delta\varepsilon$ describes the case when the thresholds for the right and left traveling waves do not agree. All the other linear coefficients of these two equations describe physical quantities, such as the relaxation time τ_0, the group velocity v_g, the linear frequency shift εc_0, the coherence length ξ_0 and the linear frequency dispersion $\xi_0^2 c_1$. All of them can be calculated from the dispersion relation $\sigma(R,q^2,k,\ldots)=\lambda\pm i\omega$ for the critical eigenvalues by the following expressions:

$$v_g=\frac{\partial\omega}{\partial q},\quad \tau_0=\frac{1}{R_c\partial\mathrm{Re}(\sigma)/\partial R},\quad c_0=R_c\tau_0\frac{\partial\omega}{\partial R},$$

$$\xi_0^2=\frac{1}{2R_c}\frac{\partial^2R}{\partial q^2},\quad c_1=-\frac{\tau_0}{2\xi_0^2}\frac{\partial^2\omega}{\partial q^2}. \tag{3.73}$$

Those derivatives are evaluated at the critical values R_c, q_c, ω_c. Typical numerical results for these physical quantities are given in Sec. IV D for representative parameter sets.

IV. NUMERICAL RESULTS

The numerical analysis of equations formulated in Secs. II and III, namely, the determination of the basic state and its instability with respect to a short wavelength secondary state,

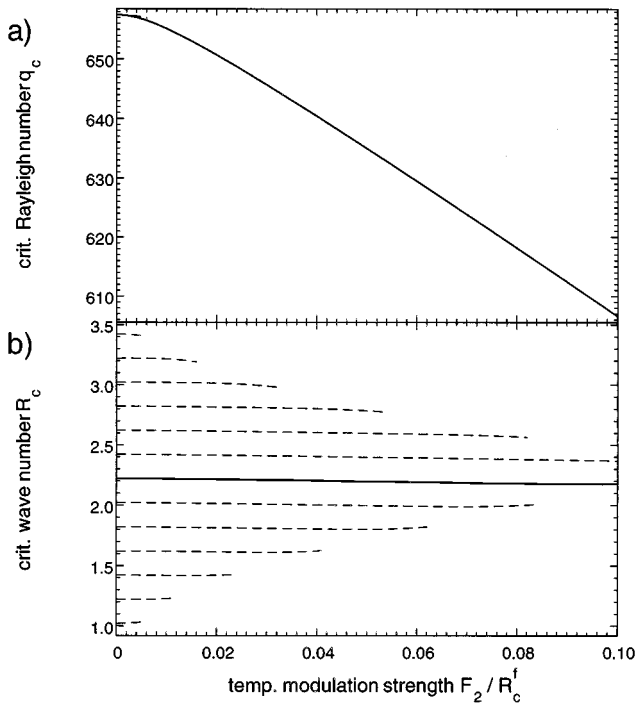

FIG. 5. The threshold for the onset of secondary flow and its critical wave number are given as a function of the normalized modulation amplitude F_2/R_c^f. The modulation wave number is $k=0.2$.

are described in the present section for a representative number of geometries and parameter combinations. Since there are no qualitative differences between the results for free and realistic rigid boundary conditions (see Sec. II B) we use stress-free boundary conditions for thermal convection in Sec. IV A for reasons of simplicity and for the rest of this section we use rigid ones. The amplitudes of the temperature modulations, F_1 and F_2, are always measured in units of the critical Rayleigh number R_c^f for stress-free boundary conditions or R_c^r for realistic boundary conditions, respectively:

$$R_c^f = 657.511, \quad R_c^r = 1707.762. \tag{4.1}$$

A. Thermal modulation of the bottom plate

The analytical expression for the basic flow in the presence of the long wavelength temperature modulation at the bottom boundary, $H_2(x)$, is given in Eq. (3.15) and its spatial structure in the x-z plane is plotted in Fig. 4.

Having in mind the relations (2.2) between the velocities v_i and the Potential Ψ it is easy to see from the lower part of Fig. 4 that the flow is upwards in the range with larger temperature differences. The amplitudes of the velocity field of the basic flow increases linearly with the amplitude of the temperature modulation and the wave number of the modulation.

The presence of the temperature modulation induces some degeneracy in the neutral curve $R_0(q)$. Instead of a single minimum in the neutral curve at q_c for the unmodulated case, one has to deal for the modulated case with several local minima that are separated by k. The location of those local minima on the neutral curve $R_0(q)$ are plotted in Fig. 5(b) for increasing values of the temperature modulation. The solid line in Fig. 5(b) indicates the absolute minimum of the neutral curve. It ends for decreasing modulation amplitudes at the local minimum q_c of the unmodulated case. The other local minima vanish for increasing values of F_2. The absolute threshold $R_c(F_2)$ decreases with increasing modulation strength as shown in Fig. 5(a). Also the critical wave number q_c decreases slightly [solid line in Fig. 5(b)]. This tendency has been also reported in the literature on similar problems [37, 39].

As a consequence of the spatial modulation of the primary flow, the envelope of the linear secondary flow at threshold is also modulated with the wave number of the temperature variation at the boundary. The modulated secondary flow is shown in Fig. 6 for two different values of the amplitude of the temperature modulation F_2. The eigenfunctions of Eq. (3.20) corresponding to the eigenvalue $\mathrm{Re}[\sigma]=0$ are shown, which are transformed via Eq. (3.19) into real space. In Fig. 6(a) the eigenfunction is given for the modulation amplitude $F_2/R_c^f=0.01$, at the critical Rayleigh number $R_c=656.25$ and the critical wave number $q_c=2.22$, and in (b) the eigenfunction is plotted for a considerably larger modulation amplitude $F_2/R_c^f=0.1$. The critical values in the latter case are already strongly reduced to $R_c=613.65$ and $q_c=2.1757$, and the eigenfunction is more localized. This strong localization of the secondary state may be sensitive to thermal fluctuations near onset.

Keeping the modulation amplitude F_2 fixed and increasing the modulation wave number k leads to increasing values for both the critical Rayleigh number R_c and the critical wave number q_c, as well as to a weaker localization of the

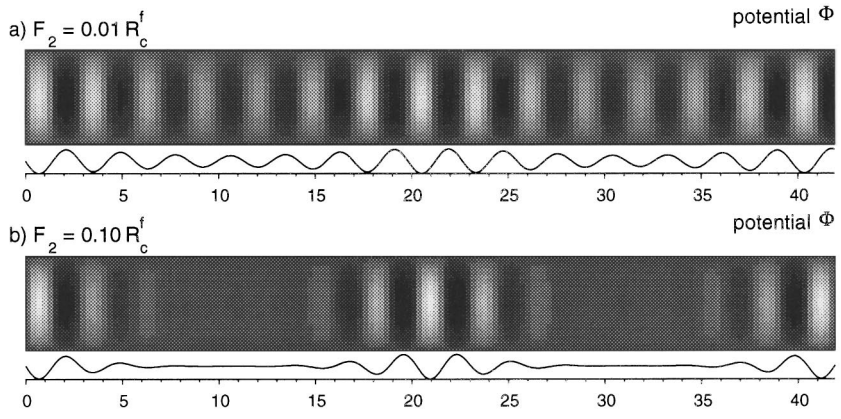

FIG. 6. The linear eigenmodes of the secondary flow are shown for the same parameters as in Fig. 4. In (a) for $F_2=0.01R_c^f$ and in (b) for $F_2=0.1R_c^f$. At the bottom of (a) and (b) now the profile for the potential of the secondary flow Φ along $z=\frac{1}{2}$ is given (stress-free boundary conditions).

linear secondary flow. This tendency persists up to commensurate ratios for q_c/k.

B. Wavy top boundary

Replacing the temperature modulation by periodic undulation of one of the boundaries, the primary flow, the spatial structure of the secondary flow as well as its critical value R_c are changed in a similar manner, as described in the previous section. The velocity field of the primary state has also a finite amplitude and it agrees with that of the boundary modulation. The critical Rayleigh number R_c at the onset of the secondary flow and the critical wave number q_c decrease again with increasing values for the undulation amplitude F_0, however, much more strongly. Increasing values for the undulation wave number k_0 lead also to increasing values for R_c and q_c. Even the localization behavior is qualitatively similar, but it is more strongly pronounced for a geometric modulation.

C. Two wavelength modulation

From the whole variety of imaginable combinations of temperature modulations at the top and bottom plates and a simultaneous periodic undulation of the top plate, we consider only a few representative configurations as described already in Sec. III B. We analyze in this section especially those modulations in more detail that show a transition into secondary drifting patterns (Sec. IV C 1) as well as a Hopf bifurcation by frustrated drifts (Sec. IV C 2).

1. Bifurcations into drifting patterns

Simultaneous modulations of the temperatures at both boundaries or an undulated top boundary combined with a temperature modulation at the bottom plate may lead to the drifting secondary flow at onset, where the drift velocity is a function of the relative phase between two modulations.

a. Two temperature modulations: $k_1=k_2$. For Rayleigh-Bénard convection with Boussinesq fluids (the only ones considered here) and modulated temperatures at the top and bottom plates with equal wave numbers, $k_1=k_2$, we find only stationary bifurcations from the primary into the secondary flow for arbitrary values between the relative phase, $\varphi_1-\varphi_2$, which is in agreement with a previous analysis [30].

b. Two temperature modulations: $k_1/k_2=2/3$. Taking commensurate ratios between the modulation wave numbers, for instance, $k_1/k_2=2/3$, then the eigenvalue spectrum of Eq. (3.67) is changed. It becomes complex for a large range of the phase differences, $\varphi_1-\varphi_2$, without having degenerate complex conjugate pairs. When the eigenvalue with the largest real part becomes critical, namely, when $\max[\mathrm{Re}(\sigma)]=0$ and $\mathrm{Im}(\sigma)=0$ are met, the corresponding critical mode is a drifting (traveling) wave with the drift velocity

$$v_D=\frac{\omega_c}{q_c}. \tag{4.2}$$

By turning the relative phase, $\varphi_1\rightarrow-\varphi_1$, the signs of ω_c and v_D are also reversed, which is different for a Hopf bifurcation, discussed below, where one has two degenerated complex conjugated eigenvalues and thus two degenerated drift directions.

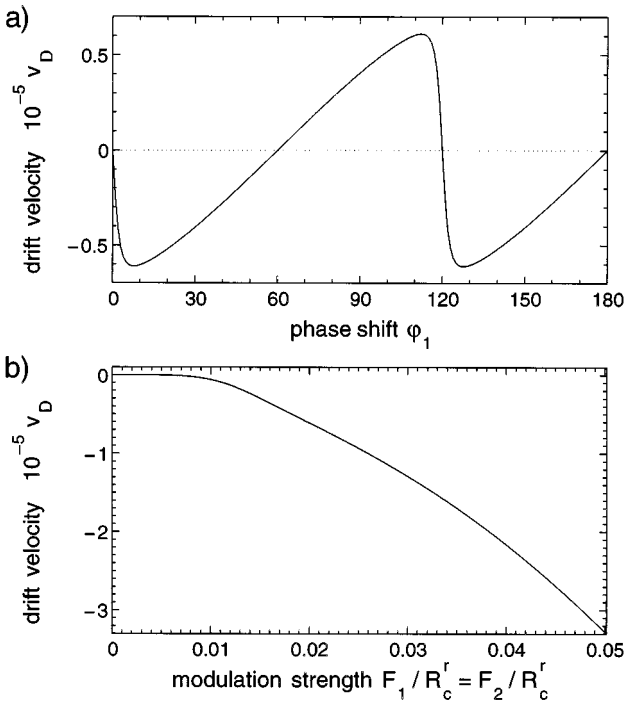

FIG. 7. The drift velocity $v_D=\omega_c/q_c$ of the secondary flow at threshold is shown in (a) as a function of the relative phase φ_1 (deg) (and $\varphi_2=0$) between the temperature modulation at the top and bottom plates. Modulation amplitudes and wave numbers have been fixed at $F_1=F_2=0.02R_c^r$ and at $k_1=2k$, $k_2=3k$ with $k=0.2$. In (b) the drift velocity v_D is shown as a function of the modulation amplitudes $F_1=F_2$ for the phases $\varphi_1=8°$ and $\varphi_2=0$.

In Fig. 7(a) the drift velocity v_D is shown as a function of the relative phase φ_1 ($\varphi_2=0$) for the wave number ratio $k_1/k_2=2/3$ and at fixed amplitudes $F_1=F_2=0.02R_c^r$, whereas in Fig. 7(b) the drift velocity is shown as a function of the modulation amplitudes and at a fixed phase difference $\varphi_1=8°$. In Fig. 7(a) the drift velocity v_D passes zero with a smaller slope at the relative phases $\varphi_1=60°, 180°, \ldots$, and changes rapidly, however, smoothly, from its maximal positive value to its negative one near the phases $\varphi_1=0°, 120°, 240°, \ldots$. Near the latter phase differences the neutral curve develops as a function of the phase difference of two neighboring minima. Both correspond to two slightly different eigenvalues in the spectrum whereas the imaginary parts of the eigenvalues and therefore the drifts v_D vanish continuously by approaching $\varphi_2=n\times120°$ ($n=0,1,2,\ldots$).

Varying the phase φ_2 at the bottom boundary instead of the phase φ_1 at the top boundary, the zeros of the drift velocities v_D are shifted from 60°,120°, . . . , to 90°,180°, . . . , and the rapid changes of v_D are shifted from 0°,120°,240°, . . . , to 180°,360°, . . . , respectively.

Drifting solutions induced by temperature modulations at both boundaries have been found earlier only for non-Boussinesq fluids, whereas for the discussed example different modulation wave numbers are enough. The situation is similar for wave number ratios $k_1/k_2=1/2$ or 2; however, as

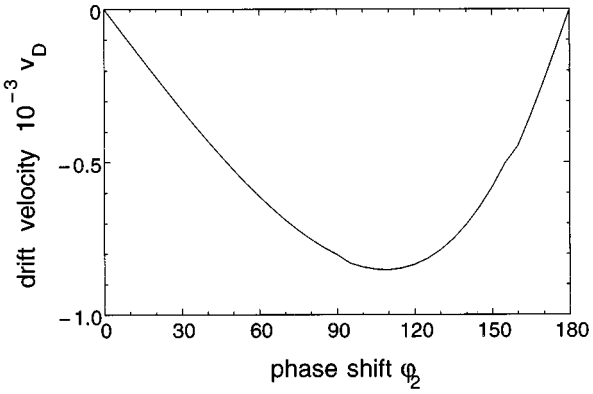

FIG. 8. The drift velocity $v_D=\omega_c/q_c$ of the secondary flow at threshold is shown as a function of the relative phase φ_2 (deg) between the temperature modulation at the bottom plate and a wavy top boundary. Modulation amplitudes have been fixed at $F_0=0.02$, $F_2=0.02R_c^r$ and the modulation wave numbers are $k_0=k_2=k=0.2$.

in the case discussed above the velocities in physical units are rather small.

c. Wavy top boundary and temperature modulation at bottom boundary: $k_0=k_2$. A wavy top boundary and a periodic temperature modulation at the bottom boundary is in various aspects equivalent to the situation of two wavy boundaries, as shown in Fig. 1. However, it is analytically and numerically much simpler.

In contrast to the temperature modulations considered in the last paragraph we observe already drifting patterns for a combination of a wavy top boundary with a temperature modulation at the bottom plate at equal wave numbers $k_0=k_2$ and finite values for the relative phase φ_2. This is shown in Fig. 8 for rigid boundary conditions, where the drift velocity of the critical eigenfunction is plotted as a function of the relative phase φ_2. In these calculations the modulation amplitudes and the wave numbers have been kept fixed at $F_0=0.02$, $F_2=0.02R_c^r$, and $k_0=k_2=0.2$. It is remarkable that the drift velocities are now three orders of magnitude larger as for two temperature modulations. The drift velocity has zeros at multiples of 180° and it is antisymmetric with respect to these zeros: $v_D(180°+\varphi_2)=-v_D(180°-\varphi_2)$. The extrema of v_D are at $\varphi_2\simeq 109°$ and at $\varphi_2\simeq 251°$, etc. for the chosen parameters. For free boundary conditions the qualitative behavior is the same, however, the absolute values for v_D are larger by a factor of about 3.

The drift velocity v_D of the critical eigenstate increases with the two modulation amplitudes F_0 and F_2 as shown in Fig. 9 at fixed values of $k_0=k_2=0.2$ and the relative phase $\varphi_2=109°$. In Fig. 10 we show additionally the dependence of the drift velocity on the modulation wave numbers $k_0=k_1=k$ and for fixed modulation amplitudes $F_0=0.02$, $F_2=0.02R_c^r$ at a fixed relative phase $\varphi_2=109°$. The nearly linear growth of $|v_D|$ with k is mainly related to the long wavelength approximation $\lambda_M\gg d$. At large values for the wave number k, $|v_D|$ is expected to be small again.

2. Hopf bifurcation by frustrated drifts

A wavy top boundary and temperature modulation at the bottom boundary with wave number ratio $k_0/k_2=3/2$, as

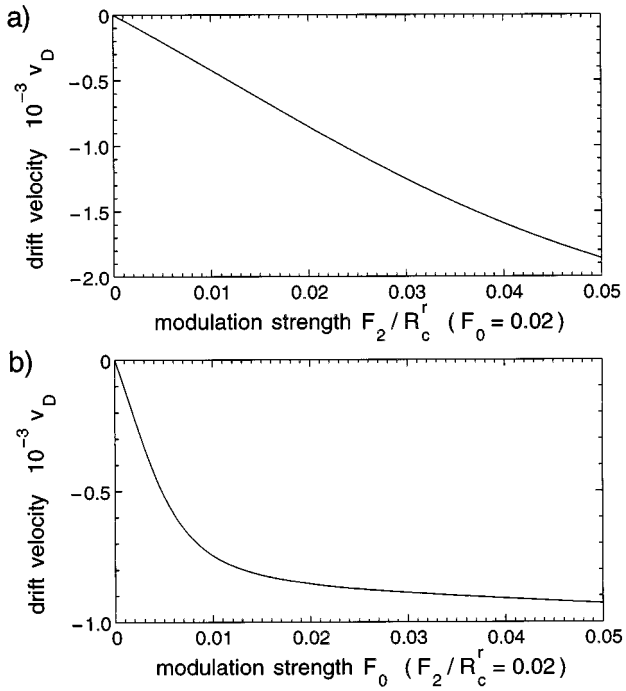

FIG. 9. The drift velocity is shown as a function of the modulations. In (a) as a function of the temperature modulation at the bottom plate F_2 at a fixed wave numbers $k_0=k_2=0.2$, phase $\varphi_2=109°$, and a geometric modulation amplitude $F_0=0.02$. In (b) as a function of the geometric modulation amplitude F_0 ($F_2=0.02R_c^r$) (rigid boundary conditions).

considered in this section, lead to a qualitatively new bifurcation scenario. As explained in the following and compared to the situations discussed above in Sec. IV C 1, the major difference is that complex conjugate pairs of eigenvalues may occur in the eigenvalue spectrum. Two of them also may become critical, in which case one has a Hopf bifurcation.

It was shown in the previous section that modulations of equal wave numbers for the undulated top boundary and the modulated bottom temperature, $k_0=k_2$, lead to a secondary state drifting either to the right ($0<\varphi_2<180°$) or to the left

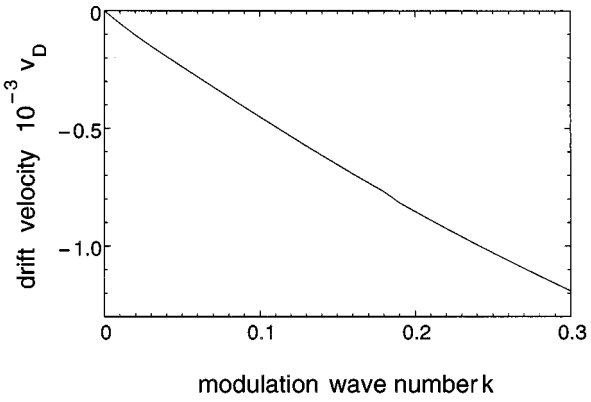

FIG. 10. The drift velocity v_D as function of the modulation wave number $k_0=k_2$ is shown, with the other parameters fixed at $F_0=0.02$, $F_2=0.02R_c^r$, $\varphi_2=109°$.

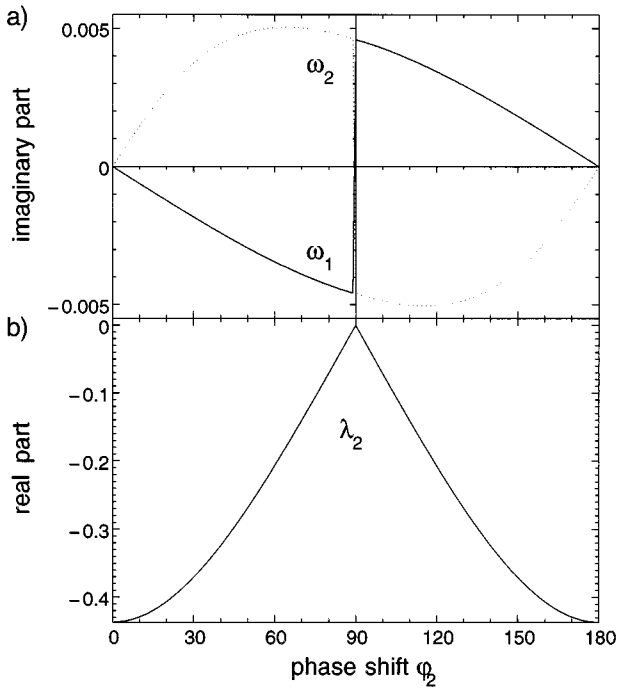

FIG. 11. In (a) the imaginary parts $\mathrm{Im}(\sigma_{1,2})$ of the two eigenvalues with the largest real parts are plotted as a function of the relative phase φ_2 (deg). In (b) the real part $\mathrm{Re}(\sigma_2)$ of the eigenvalue with the second largest real part is given. We can see that at $\varphi_2=\pm 90°$ the real parts of both eigenvalues vanish and the imaginary part has the same modulus. For these phase shifts the onset of the secondary flow takes place via a Hopf bifurcation. The following parameters have been used: modulation amplitudes $F_0=0.02$, $F_2=0.02R_c^r$ and the modulation wave numbers $k_0=2k$ and $k_2=3k$ with $k=0.2$.

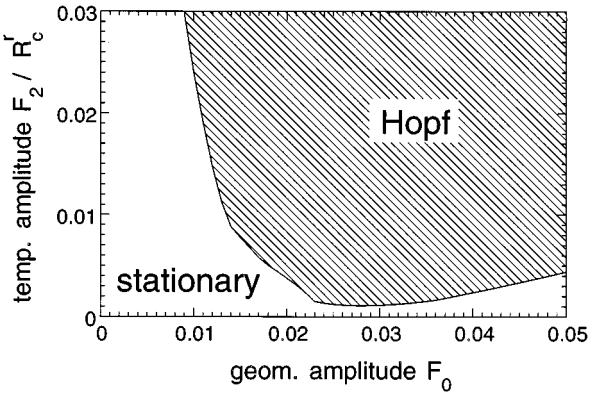

FIG. 12. In the plane of the modulation amplitudes F_0 and F_2 the ranges are indicated where the transition from the primary flow to the secondary flow takes place via a stationary or a Hopf bifurcation (shaded region). This figure indicates that finite modulation amplitudes are needed to induce a Hopf bifurcation. The ratio $k_0/k_2=2/3$ between modulation wave numbers for the wavy top boundary and the temperature modulation at the bottom boundary have been used with a relative phase $\varphi_2=90°$. Parameters: rigid boundary conditions, $k=0.2$, $k_0=2k$, and $k_2=3k$.

$(180°<\varphi_2<360°)$, such as indicated in Fig. 8. In these cases the secondary state is drifting for rather arbitrary values for the amplitudes F_0, F_2 and modulation wave number k. Only at phases $\varphi_2=0°,180°,\ldots$, the bifurcation from the primary state is stationary and the imaginary part ω_i as well as the drift velocity changes its sign by passing these values.

Changing the phase φ_2 for the wave number ratio $k_2/k_0=3/2$, the secondary state occurs via a right drifting pattern for phases, $0<\varphi_2<90°$, and via a left drifting pattern for $90°<\varphi_2<180°$. This is indicated in Fig. 11(a) where the imaginary parts $\omega_{1,2}=\mathrm{Im}(\sigma_{1,2})$ of the two eigenvalues with the largest real parts are plotted. In Fig. 11(b) the second largest real part, $\lambda_2=\mathrm{Re}[\sigma_2]$, is given, while the largest real part is kept critical, $\max \mathrm{Re}[\sigma]=0$, by adjusting R to R_c.

The moduli of the imaginary parts of both eigenvalues (ω_i) increase with φ_2 and become equal at $\varphi_2=90°,270°,\ldots$. At these phases the real part of the second largest eigenvalue vanishes too $(\mathrm{Re}[\sigma_1]=0=\mathrm{Re}[\sigma_2])$ and the bifurcation from the primary flow into the secondary flow is oscillatory with two degenerated complex-conjugated eigenvalues. One has a Hopf bifurcation at this crossing point. This Hopf bifurcation is a rather novel phenomenon, which has been predicted recently for a model [52]. We call this phenomenon *Hopf bifurcation induced by frustrated drifts*, because at these values both drift directions have the same threshold and thus there is no uniquely preferred drift direction anymore. Immediately above threshold the nonlinear interaction between both drift directions favors a superposition of both linear drifting modes and one has standing waves [62].

The sign of the drift velocity v_D changes abruptly at $90°,270°,\ldots$ by the interchange of the two critical complex eigenvalues. The transition into the secondary flow becomes stationary $(v_D=0)$ at $\varphi_2=0°,180°,\ldots$ and ω, as well as the drift velocity v_D, changes its sign smoothly at these values, as indicated in Fig. 11(a).

The degeneracy of two critical complex conjugate eigenvalues at $\varphi=90°,270°,\ldots$ (Hopf bifurcation by frustrated drifts) does not occur at arbitrary combinations of F_0, F_2, and k. Moreover, as indicated in Figs. 12 and 13 these parameters have to be beyond certain thresholds. In Fig. 12 the phase $\varphi_2=90°$ and the wave numbers are fixed: $k_0=2k$, $k_2=3k$, $k=0.2$. The amplitudes F_0,F_2 are varied, whereby the Rayleigh number has been always adjusted appropriately to reach the critical point $\max \mathrm{Re}[\sigma_i]=0$. The shaded region indicates the amplitude combinations F_0, F_2, where the transition from the primary into the secondary flow happens via a Hopf bifurcation by frustrated drifts. Otherwise the transition is stationary. In Fig. 13 $F_0=0.02$ is kept fixed and F_2 as well as the modulation wave number k are scanned. Again rigid boundary conditions and the wave number ratio $k_0/k_2=2/3$ have been used. At very small and at larger values of k the Hopf bifurcation disappears. In that sense there is also a threshold for the modulation wave number.

The phase boundaries in Figs. 12 and 13 are not smooth everywhere, because the neutral curve has several local minima separated by k, as indicated for a special case in Fig. 5. When parameters are changed, the absolute one of these local minima is not always the same—on the stationary as well as on the Hopf branch. At parameters where the absolute minimum of the neutral curve changes its position in k

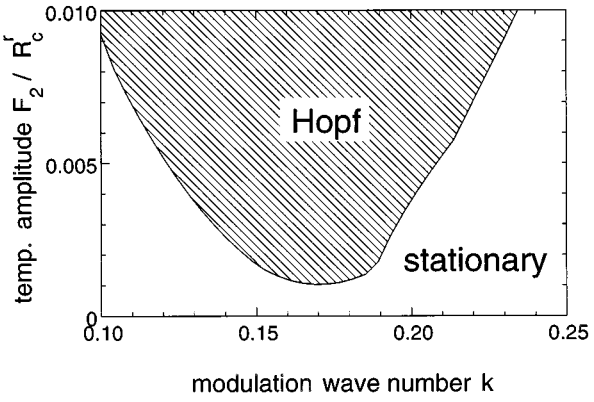

FIG. 13. At parameters in the shaded range the transition from the primary to the secondary flow takes place via a Hopf bifurcation. The geometric undulation amplitude was fixed at $F_0=0.02$, the wave numbers at $k_0=2k$, $k_2=3k$, and the phase at $\varphi_2=90°$. The amplitude of the temperature modulation is given in units of the critical Rayleigh number of the unmodulated case $R_c^r=1708$ (rigid boundary conditions).

space (from one local minimum to another one), then a discontinuity for the tangent of the phase boundaries might occur, as can be seen for a few positions at the phase boundary in Figs. 12 and 13.

For a fixed amplitude $F_0=0.02$ we show in Fig. 14 the eigenfunctions of the secondary flow at three different values of F_2 ($\varphi_2=90°$ and $k=0.2$). In Fig. 14(a) the velocity potential of the secondary flow at onset, Φ, is shown for a stationary bifurcation at parameters just outside the shaded region in Fig. 12. In Fig. 14(b) Φ is shown for a localized traveling wave state at onset of the secondary flow for a parameter set just above the separation line and in Fig. 14(c) far inside the shaded region of Fig. 12. All three states are plotted for the length $L=2\pi/k$. In the case of traveling wave states the envelope is fixed and the phase is traveling.

There is a significant difference between the eigenstate on the stationary and the Hopf branch. The eigenfunction at the stationary branch has two periods on the length L, as shown in Fig. 14 and the oscillatory state has only one spatial period on the same length L. The stationary bifurcation is therefore harmonic with respect to the smaller of the external modulations, $k_0=2k$, and the oscillatory one is subharmonic with respect to k_0. The opposite traveling wave state is also localized in space and subharmonic, however, translated in space by $L/4$. The subharmonic behavior is an essential signature of the Hopf bifurcation by frustrated drifts. This is in contrast to the drifting solutions discussed in Sec. IV C 1, where all solutions were harmonic with respect to the smallest external wave number.

3. Codimension-2 bifurcation

At the phase boundaries in Figs. 12 and 13 there is an interesting competition between a stationary and an oscillatory instability, a so-called codimension-2 bifurcation [63], which we analyze in more detail in this section. For that purpose the phase $\varphi_2=\pi/2$ between the two modulations and the ratio, $k_0/k_2=2/3$, are kept fixed.

It is already indicated in Fig. 5 for a simpler case that the neutral curves for the stationary (st) and the Hopf branch (H) may have several local minima—also near the phase boundaries in Figs. 12 and 13. The location of five such local minima on the stationary branch are plotted in Fig. 15(b) as a function of the temperature modulation F_2 and for parameters near phase boundary in Fig. 12. The respective thresholds are given in Fig. 15(a) whereby $k=0.2$ and $F_0=0.02$ have been kept fixed. The solid line in Fig. 15 corresponds to the Hopf branch. The local minima on the stationary branch are separated roughly by the wave number k. With increasing values of F_2 the minima of the neutral curve at $q_c^{st}\approx 3.25$ and at $q_c^{st}\approx 2.92$ become narrower and narrower and then coalesce to a Hopf branch with a higher threshold than the lowest stationary one.

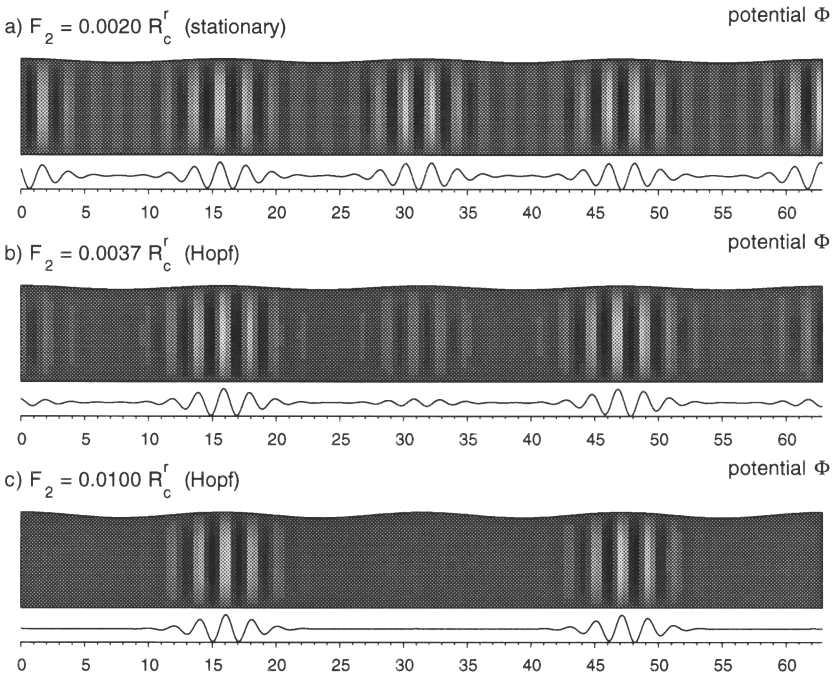

FIG. 14. The velocity potential Φ at the onset of the secondary state is shown. In (a) the form of the eigenstate Φ is shown in the stationary regime, in (b) just inside the Hopf regime (indicated in Fig. 12), and in (c) deep in the Hopf regime. $k=0.2, F_0=0.02$, and $\varphi_2=90°$ have been used. The horizontal length in the figure is $L=2\pi/k$. The stationary eigenstate in (a) has two periods in between this length and the oscillatory states, shown in (b) and (c), have one period on the given length L. Therefore the stationary state is harmonic with respect to the modulation wave number $k_0=2k$ and the oscillatory ones are subharmonic.

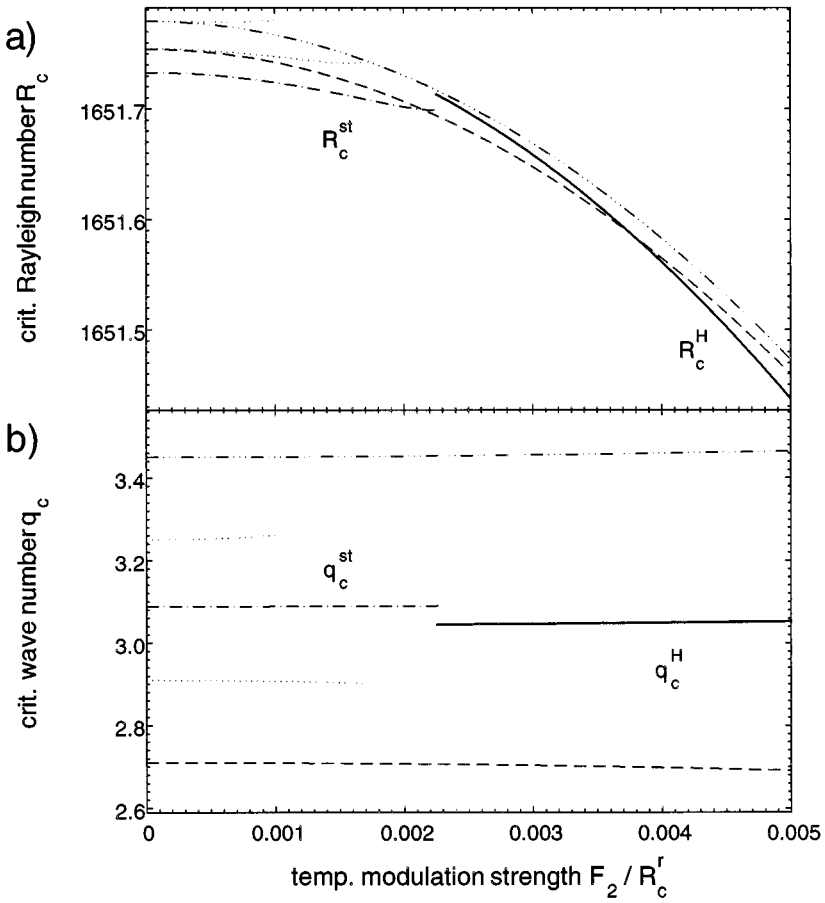

FIG. 15. In (a) the thresholds $R_c^{st,H}$ and in (b) the critical wave numbers $q_c^{st,H}$ at the local minima of the stationary bifurcation branches (dashed-dotted lines) and the Hopf bifurcation (solid line) are shown as a function of the amplitude of the thermal modulation at the bottom plate F_2. The rest of the parameters have been fixed at the same values as in Fig. 12.

The local minimum on the stationary branch at $q_c^{st} \approx 3.09$ is the absolute minimum for small values of F_2. Increasing the amplitude F_2 then near $F_2 \approx 0.0022 R_c^f$ the local minimum at $q_c^{st} \approx 2.72$ becomes the absolute minimum of the neutral curve. At even larger values for $F_2 > F_{2c} \approx 0.00378 R_c^f$ the Hopf branch (solid line) in Fig. 15 becomes the absolute minimum, with a lower threshold than the lowest minimum at $q_c^{st} \approx 2.72$ of the stationary branch. This latter exchange of stability takes place at the phase boundaries shown in Figs. 12 and 13. Near $F_2 \approx 0.0022 R_c^f$ two stationary instabilities with different wavelength are competing (dashed and dashed-dotted). The nonlinear interaction between both modes may give rise to interesting phenomena near the phase boundaries in Figs. 12 and 13.

Since we are focusing mainly on the occurrence of the Hopf bifurcation by frustrated drifts, we show in Fig. 16 the structure of the neutral curve in more detail near the phase boundary for three different values of F_2, around the codimension-2 value $F_{2c} \approx 0.00378 R_c^f$. The dashed lines are neutral curves belonging to the stationary branch with the two local minima located at $q^{st} \approx 3.44$ and $q^{st} \approx 2.71$ in Fig. 15(b). The solid line is the neural curve of the Hopf branch. In Fig. 16(a) the neutral curves are shown for $F_2 = 0.0025 < F_{2c}$ below the codimension-2 point (CTP), in Fig. 16(b) at the CTP, $F_2 = F_{2c}$, and in Fig. 16(c) beyond the CTP at $F_2 = 0.01 > F_{2c}$. Starting from F_{2c} and decreasing F_2 then the q range of the Hopf branch becomes narrower and vanishes in a complex manner near some finite value for $F_2 \approx 0.0023 R_c^r$.

Whenever the solid line in Fig. 16 terminates at the neutral curves of the stationary branches (dashed lines) the Hopf frequency ω_0 vanishes and one has a double-zero eigenvalue. This behavior is very similar to the codimension-2 bifurcation occurring in binary fluid convection [59, 64]. Apart from two nearly critical eigenvalues in the vicinity of F_{2c} (F_0 and k fixed) all other eigenvalues have strongly negative real parts and are damped. In this situation the n-order characteristic polynomial, equivalent to Eq. (3.67), can be separated into one of the order $n-2$ and into a further one of second order:

$$\sigma^2 - e(R,q)\sigma - d(R,q) = 0 \,. \tag{4.3}$$

This reduced polynomial describes the dynamics of the two nearly critical eigenvalues in the vicinity of the codimension-2 point F_{2c}. With the arguments following Eq. (3.23) the conditions $e=0$ and $d=0$ give the neutral curves $R_0^{osc}(q)$ and $R_0^{stat}(q)$, respectively. A similar approach as been used to describe the codimension-2 bifurcation in binary fluid convection. For that situation also a generalized amplitude equation has been derived [64], which reproduces the dispersion relation given in Eq. (4.3) for a special case. From the nonlinear analysis of that equation interesting dynamical behavior has been found near such codimension-2 bifurcations [63, 64].

The essential features of the neutral curves shown in Fig. 16 can be reproduced by a second order polynomial given in Eq. (4.3) with the explicit expressions for the coefficients:

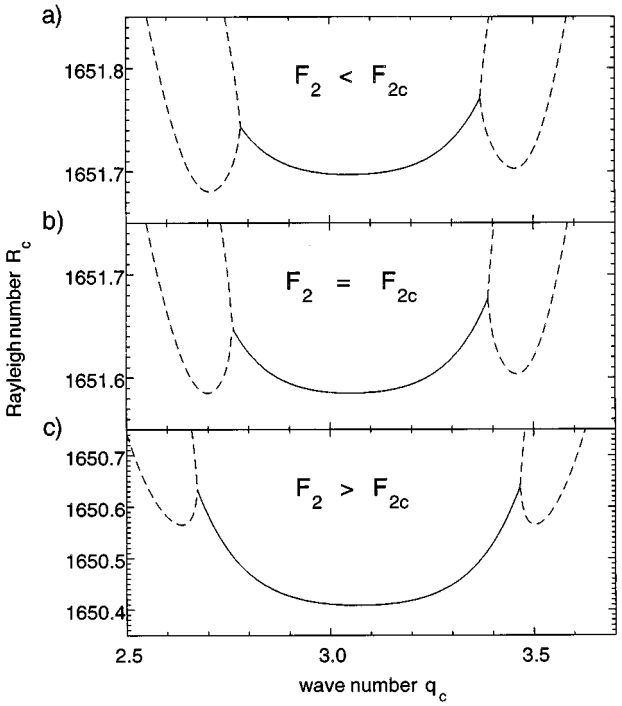

FIG. 16. The neutral curves for the stationary bifurcation $R_0^{\mathrm{st}}(q)$ (dashed line) and for the Hopf bifurcation $R_0^H(q)$ (solid line) are shown for three different values of the thermal modulation amplitude F_2, whereas the rest of the parameters are kept fixed at the same values as in Fig. 15. In (a) $F_2=0.0025R_c^r<F_{2_c}$ in (b) $F_2=F_{2_c}=0.0037R_c^r$, and in (c) $F_2=0.01R_c^r>F_{2_c}$. The Hopf frequency always vanishes when the Hopf branch (solid line) meets the stationary branch (dashed line).

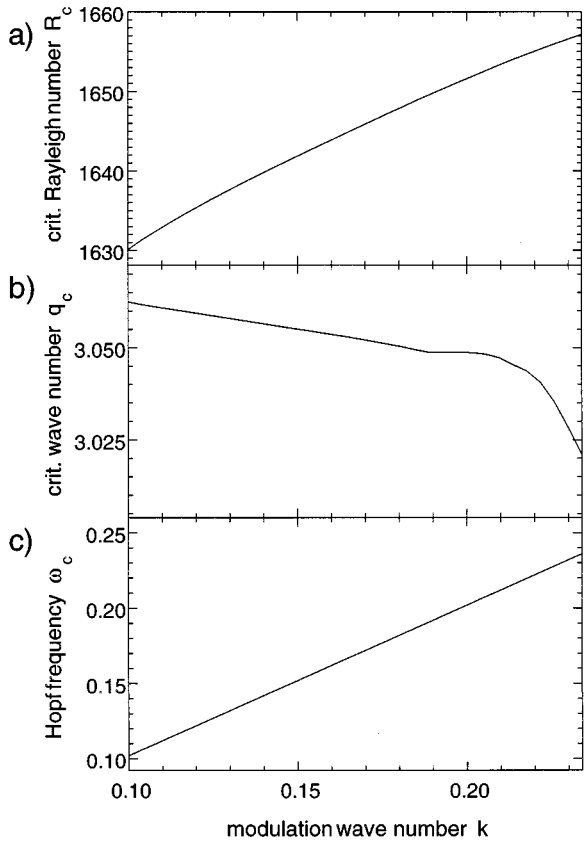

FIG. 17. In (a) the critical Rayleigh number R_c, in (b) the critical wave number q_c^H, and in (c) the Hopf frequency ω_c for parameters along the solid line in Fig. 13 are shown.

$$e(R,Q)=\varepsilon-\beta Q^2, \tag{4.4}$$

$$d(R,Q)=\varepsilon-\eta-\frac{\alpha^2}{4}+\alpha Q^2-\gamma Q^4, \tag{4.5}$$

with

$$Q=q-q_c^H,$$

$$\alpha\approx 8(q_c^{\mathrm{st}}-q_c^H)^2, \quad \eta\propto F_2-F_{2c}.$$

Herein β reflects the curvature of the neutral curve at the Hopf branch and γ is a free parameter to fix the form of the neutral curve for the stationary branch as close as possible. From $\sigma=d=0$ the neutral curve for the stationary branch can be determined, which has obviously two minima. The two minima of the neutral curve of the stationary branch are the essential difference from the polynomial discussed earlier in the context of binary fluid convection [59, 64]. The modified corresponding generalized amplitude equation is discussed elsewhere.

Along the phase boundaries in Figs. 12 and 13, the critical quantities at the Hopf branch, the critical Rayleigh number R_c^H, the critical Hopf frequency ω_c, and the critical wave number q_c^H vary only slightly. This is shown explicitly in Fig. 17 where those quantities are given along the phase boundary in Fig. 13. Therefore one expects similar bifurcation behavior wherever one crosses the phase boundaries in Figs. 12 and 13.

D. Linear coefficients of the amplitudes equations above the Hopf bifurcation

The coefficients in the amplitude equations defined in Sec. III C describe the physical quantities such as the Hopf frequency ω_c, relaxation time τ_0, coherence length ξ_0, linear frequency shift εc_0, group velocity v_g, and linear frequency dispersion $\xi_0^2 c_1$. These characterize the linear properties of the patterns near threshold to a great extent. Hence, we have plotted them in Fig. 18 for a typical parameter set as a function of the modulation amplitude F_2 (other parameters are the same as in Fig. 16). Below F_{2c} (dotted lines) the quantities correspond to the coefficients of the stationary bifurcation and beyond F_{2c} to the coefficients of the amplitude equation near a Hopf bifurcation. The discontinuity of the coherence length ξ_0 [Fig. 18(e)] reflects the exchange of the absolute minimum of the neutral curve from one local minimum to another, which have different curvatures at the minimum.

V. SUMMARY AND CONCLUSION

Our quantitative analysis gives an estimate where the phenomenon of Hopf bifurcation by frustrated drifts, predicted

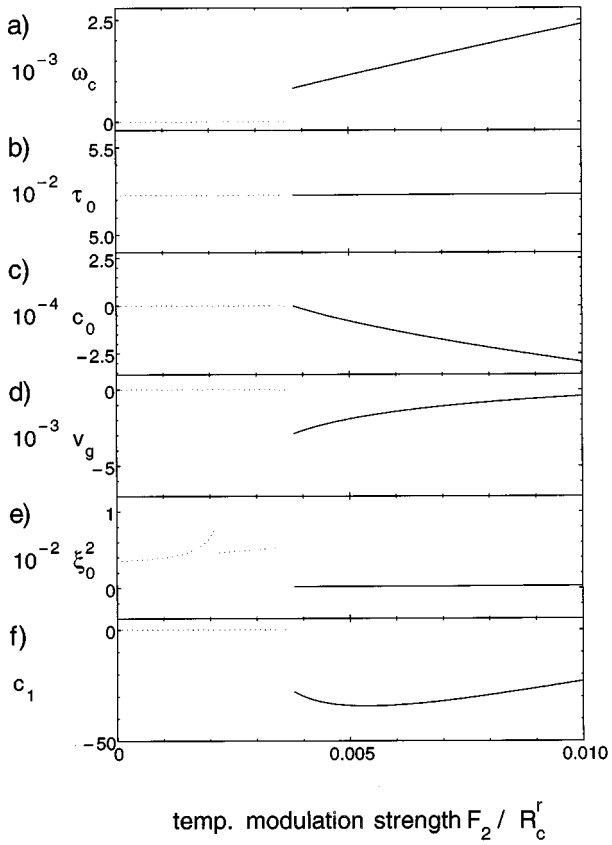

FIG. 18. Coefficients of amplitude equation (3.72) as a function of the modulation amplitude F_2. The other parameters are the same as in Fig. 15. The dotted lines are the physical quantities below F_{2c} on the stationary branch and beyond F_{2c} for the Hopf branch, which are indicated by the solid lines.

for a model system [52], can be expected in experiments on Rayleigh-Bénard convection with modulated boundaries. We did our calculations in the limit of large Prandtl numbers (approximately valid, for instance, for olive oil). However, a preliminary work shows that finite values for the Prandtl number will change the effects only quantitatively.

In the present work have we analyzed the onset of secondary convection for temperature modulations at one or at two boundaries (top and bottom) alone as well as in combination with an undulated top boundary. While we found patterns drifting in a specific direction for temperature modulations at both boundaries alone, we find a Hopf bifurcation by frustrated drifts only when an undulated boundary is combined with a temperature modulation at the same or the opposite boundary. Choosing an undulated bottom boundary in combination with a temperature modulation at the top boundary gives the same results, only the actual numbers for the relative phases are shifted where the various transitions take place. For two undulated boundaries without temperature modulations we expect qualitatively similar results whenever we have not considered this case explicitly in our calculations.

In our approach we made no assumption about the strength of the modulation amplitudes F_i. However, it turns out that the central phenomenon of this work, the Hopf bifurcation by frustrated drifts, occurs already for relatively small modulation amplitudes. Thus, this observation seems to justify a perturbation expansion with respect to small values for the modulation wave numbers k_i (as we did already here) and with respect to small modulation amplitudes F_i. Accordingly, we are applying a perturbation approach [58, 65] to our problem in a forthcoming work, where we describe the derivation of a generalized Ginzburg-Landau equation including the external modulations [52, 66]. The preliminary analysis shows that the onset of the secondary flow, calculated in terms of this generalized amplitude equation, agrees very well with the results presented here [52]. Furthermore, the analysis of the amplitude equation shows that the onset of the secondary convection via Hopf bifurcation by frustrated drifts is supercritical and standing waves are the preferred state beyond the bifurcation. This is different from several other real systems, such as, for instance, in convection in binary fluids, where the Hopf bifurcation is subcritical [59, 67]. Tertiary bifurcation from standing waves into further structures is also covered by that generalized Ginzburg-Landau equation.

In contrast to Boussinesq fluids considered in this work, in non-Boussinesq fluids Hopf bifurcation by frustrated drifts can be expected even for flat boundaries with modulations of the temperatures at the top and bottom boundaries [62].

Drifting patterns induced by broken symmetries occur also in electroconvection in nematic liquid crystals [68–71], where the symmetry is broken by a pretilt angle between the orientational field in nematic liquid crystals (the director field) and the top or bottom boundary. Within a model equation, which covers the essential symmetries for electroconvection in nematic liquid crystals with spatially periodic pretilt, it was shown that Hopf bifurcation by frustrated drifts can also be expected in that system [72]. While the Hopf bifurcation by frustrated drifts was investigated in the present work for a quasi-one-dimensional situation, also interesting orientational oscillations of convection rolls are predicted for two-dimensional anisotropic systems [72].

Another experimentally interesting configuration is the wave number ratio $k_2/k_0=2$. For this ratio one obtains similar scenarios for Hopf bifurcation by frustrated drifts at slightly different relative phases and modulation amplitudes. The detailed results of this case will be described elsewhere.

One can imagine further interesting nonlinear phenomena related to Hopf bifurcation by frustrated drifts, especially for well-defined periodic pretilt configurations in electroconvection in nematics. An essential point for the occurrence of all such dynamical phenomena induced by frustrated drifts is the interplay between two types of periodic structures, one with a large wavelength and the other one with a short wavelength. In electroconvection the interaction of a pattern of short wavelength with one of long wavelength occurs spontaneously beyond secondary bifurcations [51, 73]. The resulting dynamic structures of defect lattices and chevrons exhibit also dynamic behavior. Thus, it is very likely that dynamic behavior of patterns, as discussed in the present work, are a generic result of interactions between patterns of very different wave numbers.

ACKNOWLEDGMENTS

We are grateful to H. Müller-Krumbhaar for useful discussions and to the German science foundation (DFG) for financial support.

APPENDIX: TRANSFORMATION TO FLAT BOUNDARIES

The partial derivatives, ∂_x, ∂_z, take the following form in terms of the new coordinates, ξ, η, according to the transformation (3.27):

$$\partial_z = A\partial_\eta, \quad \partial_x = \partial_\xi + \eta B \partial_\eta. \tag{A1}$$

[$A(\xi)$ and $B(\xi)$ are defined in Eqs. (3.29) and (3.32).] $B(\xi)$ is of first order in the modulation wave number k. This allows in the limit of small values of k a considerable simplification of the transformation of higher-order derivatives ∂_x^n:

$$\partial_x^n = \partial_\xi^n + n\,\eta B \partial_\xi^{n-1}\partial_\eta + O(k^2). \tag{A2}$$

The derivatives with respect to z transform as

$$\partial_z^n = A^n \partial_\eta^n. \tag{A3}$$

Therefore the transformed Laplacian Δ is up to the leading order $O(k)$ of the form

$$\Delta = \partial_\xi^2 + A^2\partial_\eta^2 + 2\,\eta B \partial_\xi \partial_\eta + O(k^2). \tag{A4}$$

Similarly one obtains

$$\Delta^2 = \partial_\xi^4 + A^4\partial_\eta^4 + 4\,\eta B \partial_\xi^3 \partial_\eta + 2A^2\partial_\xi^2\partial_\eta^2 + 8A^2 B \partial_\xi \partial_\eta^2 + 4A^2 B\,\eta \partial_\xi \partial_\eta^3 + O(k^2). \tag{A5}$$

[1] H. Bénard, Gén. Sci. Pures Appl. **11**, 1261 (1900); **11**, 1309 (1900).
[2] L. Rayleigh, Philos. Mag. **32**, 529 (1916).
[3] S. Chandrasekhar, *Hydrodynamic and Hydromagnetic Stability* (Oxford University Press, London, 1961).
[4] F. H. Busse, in *Hydrodynamic Instabilities and the Transition to Turbulence*, Topics in Applied Physics Vol. 45, edited by H. L. Swinney and J. P. Gollub (Springer, New York, 1981).
[5] *Propagation in Systems far from Equilibrium*, edited by J. E. Wesfreid *et al.* (Springer, New York, 1988).
[6] *New Trends in Nonlinear Dynamics and Pattern-Forming Phenomena: The Geometry of Nonequilibrium*, edited by P. Coullet and P. Huerre (Plenum, New York, 1990).
[7] *Nonlinear Evolution of Spatio-Temporal Structures in Dissipative Continuous Systems*, edited by F. H. Busse and L. Kramer (Plenum, New York, 1990).
[8] D. Campbell, R. Ecke, and J. M. Hyman, *Nonlinear Science: The Next Decade*, special issue of Physica D **51** (1991).
[9] *Pattern Formation in Complex Dissipative Systems*, edited by S. Kai (World Scientific, Singapore, 1992).
[10] *Spatio-Temporal Patterns in Nonequilibrium Complex Systems*, Vol. XXI of *Santa Fe Institute Studies in the Sciences of Complexity*, edited by P. Cladis and P. Palffy-Muhoray (Addision-Wesley, New York, 1995).
[11] I. Rehberg *et al.*, Phys. Rev. Lett. **67**, 596 (1991).
[12] W. Schöpf and I. Rehberg, Europhys. Lett. **17**, 321 (1992).
[13] G. Quentin and I. Rehberg, Phys. Rev. Lett. **74**, 1578 (1995).
[14] M. Wu, G. Ahlers, and D. S. Cannell, Phys. Rev. Lett. **75**, 1743 (1995).
[15] M. C. Cross, P. G. Daniels, P. C. Hohenberg, and E. D. Siggia, J. Fluid Mech. **55**, 155 (1983).
[16] M. M. Chen and J. A. Whitehead, J. Fluid Mech. **31**, 1 (1968).
[17] K. Stork and U. Müller, J. Fluid Mech. **54**, 599 (1972).
[18] M. C. Cross, Phys. Rev. A **25**, 1065 (1982).
[19] S. Zaleski, Y. Pomeau, and A. Pumir, Phys. Rev. A **29**, 366 (1984).
[20] M. C. Cross, Phys. Rev. A **38**, 3593 (1988).
[21] V. Steinberg, J. Fineberg, E. Moses, and I. Rehberg, Physica D **37**, 359 (1989).
[22] P. Kolodner, C. M. Surko, and H. Williams, Physica D **37**, 319 (1989).
[23] F. Zhong, R. E. Ecke, and V. Steinberg, Phys. Rev. Lett. **67**, 2473 (1991).
[24] L. Ning and R. E. Ecke, Phys. Rev. E **47**, R2991 (1993).
[25] E. Y. Kuo and M. C. Cross, Phys. Rev. E **47**, 2245 (1993).
[26] L. Kramer, E. Ben-Jacob, H. R. Brand, and M. C. Cross, Phys. Rev. Lett. **49**, 1891 (1982).
[27] D. S. Cannell, M. A. Dominguez-Lerma, and G. Ahlers, Phys. Rev. Lett. **50**, 1365 (1983).
[28] L. Kramer and H. Riecke, Z. Phys. B **59**, 245 (1985).
[29] I. Rehberg, E. Bodenschatz, B.Winkler, and F. H. Busse, Phys. Rev. Lett. **59**, 282 (1987).
[30] G. Hartung, F. H. Busse, and I. Rehberg, Phys. Rev. Lett. **66**, 2741 (1991).
[31] M. Belzons *et al.*, Europhys. Lett. **4**, 909 (1987).
[32] P. Devillard, F. Dunlop, and B. Souillard, J. Fluid Mech. **186**, 521 (1988).
[33] W. Zimmermann, M. Sesselberg, and F. Petruccione, Phys. Rev. E **48**, 2699 (1993).
[34] L. Howle, R. P. Behringer, and J. Georgiades, Nature **362**, 230 (1993).
[35] D. M. Shattuck, R. P. Behringer, G. A. Johnson, and J. G. Georgiadis, Phys. Rev. Lett. **75**, 1934 (1995).
[36] J. Tavantzis, E. L. Reiss, and B. J. Matkowsky, SIAM J. Appl. Math. **34**, 322 (1978).
[37] R. E. Kelly and D. Pal, J. Fluid Mech. **86**, 433 (1978).
[38] P. Coullet and P. Huerre, Physica D **23**, 27 (1986).
[39] D. A. S. Rees and D. S. Riley, J. Fluid Mech. **166**, 503 (1986).
[40] D. A. S. Rees and D. S. Riley, J. Fluid Mech. **199**, 133 (1989).
[41] D. A. S. Rees and D. S. Riley, Proc. R. Soc. London Ser. A **421**, 303 (1989).
[42] M. Lowe, J. P. Gollub, and T. Lubensky, Phys. Rev. Lett. **51**, 786 (1983).
[43] M. Lowe and J. P. Gollub, Phys. Rev. A **31**, 3893 (1985).
[44] M. Lowe, B. S. Albert, and J. P. Gollub, J. Fluid Mech. **173**, 253 (1986).
[45] P. Coullet, Phys. Rev. Lett. **56**, 724 (1986).
[46] P. Coullet and D. Repaux, Europhys. Lett. **3**, 573 (1987).
[47] L. Gil *et al.*, Phys. Rev. Lett. **66**, 3249 (1991).
[48] A. Ogawa, K. Kawasaki, W. Zimmermann, and T. Kawakatsu, in *Dynamics and Patterns in Complex Fluids*, edited by A.

Onuki and K. Kawasaki (Springer, Berlin, 1990), p. 78.
[49] W. Zimmermann *et al.*, Europhys. Lett. **24**, 217 (1993).
[50] A. Ogawa, W. Zimmermann, K. Kawasaki, and T. Kawakatsu, J. . Phys. (France) II **6**, 305 (1996).
[51] S. Nasuno, O. Sasaki, S. Kai, and W. Zimmermann, Phys. Rev. A **46**, 4954 (1992).
[52] W. Zimmermann and R. Schmitz, Phys. Rev. E **53**, 1321 (1995).
[53] W. Zimmermann and R. Schmitz, in *Spatio-Temporal Patterns in Nonequilibrium Complex Systems*, edited by P. Cladis and P. Palffy-Muhoray (Addison-Wesley, New York, 1994).
[54] R. Schmitz, Diploma thesis, RWTH Aachen, 1993 (unpublished).
[55] F. H. Busse, Rep. Prog. Phys. **41**, 1929 (1978).
[56] A. Schlüter, D. Lortz, and F. H. Busse, J. Fluid Mech. **23**, 129 (1965).
[57] H. R. Brand, P. Lomdahl, and A. C. Newell, Physica D **23**, 345 (1986).
[58] A. C. Newell, T. Passot, and J. Lega, Annu. Rev. Fluid Mech. **25**, 399 (1992).
[59] W. Schöpf and W. Zimmermann, Phys. Rev. E **47**, 1739 (1993).
[60] P. Coullet, S. Fauve, and E. Tirapequi, J. Phys. (Paris) Lett. **46**, L787 (1985).
[61] M. C. Cross, Phys. Rev. Lett. **57**, 2935 (1986).
[62] R. Schmitz and W. Zimmermann (unpublished).
[63] J. Guckenheimer and P. Holmes, *Nonlinear Oscillations, Dynamical Systems, and Bifurcations of Vector Fields* (Springer, Berlin, 1983).
[64] W. Zimmermann, D. Armbruster, L. Kramer, and W. Kuang, Europhys. Lett. **6**, 505 (1988).
[65] M. C. Cross and P. C. Hohenberg, Rev. Mod. Phys. **65**, 851 (1993).
[66] W. Zimmermann and R. Schmitz (unpublished).
[67] W. Schöpf and W. Zimmermann, Europhys. Lett. **8**, 41 (1989).
[68] V. A. Raghunathan, P. R. M. Murthy, and N. V. Madhusudana, Mol. Cryst. Liq. Cryst. **199**, 239 (1991).
[69] W. Zimmermann, in *Defects, Singularities in Nematic Liquid Crystals: Mathematical and Physical Aspects*, Vol. 332 of *NATO Advanced Study Institute, Series C*, edited by J. M. Coron, J. M. Ghidaglia, and F. Helein (Kluwer, Dordrecht, 1991), p. 401.
[70] O. Ahmetshin, V. Delev, and O. Scaldin, Mol. Cryst. Liq. Cryst. **265**, 315 (1995).
[71] A. Hertrich, A. Krekhov, and W. Pesch, J. Phys. (France) II **5**, 733 (1995).
[72] R. Schmitz and W. Zimmermann (unpublished).
[73] S. Kai and W. Zimmermann, Prog. Theor. Phys. Suppl. **99**, 458 (1989).